Dalton Transactions

PAPER

View Article Online
View Journal | View Issue

Cite this: *Dalton Trans.*, 2016, **45**, 8622

Postsynthetic modifications of [2,2,2-(H)(PPh$_3$)$_2$-*closo*-2,1-RhSB$_8$H$_8$] with Lewis bases: cluster modular tuning†

Susana Luaces,[a] Vincenzo Passarelli,[a,b] María José Artigas,[a] Fernando J. Lahoz,[a] Luis A. Oro[a] and Ramón Macías*[a]

Received 3rd March 2016,
Accepted 18th April 2016

DOI: 10.1039/c6dt00856a

www.rsc.org/dalton

It has been demonstrated that the reaction of [2,2,2-(H)(PPh$_3$)$_2$-*closo*-2,1-RhSB$_8$H$_8$] (**1**) with PPh$_3$ affords the boron substituted rhodathiaborane–PPh$_3$ adduct, [6,6-(PPh$_3$)$_2$-9-(PPh$_3$)-*arachno*-6,5-RhSB$_8$H$_9$] (**2**). Building upon this reaction, we report herein that the 10-vertex hydridorhodathiaborane **1** reacts with the Lewis bases, PCy$_3$, py, 2-Mepy, 2-Etpy, 3-Mepy and 4-Mepy to form the rhodathiaborane–ligand adducts, [6,6-(PPh$_3$)$_2$-9-(L)-*arachno*-6,5-RhSB$_8$H$_9$], where L = PCy$_3$ (**3**), 2-Mepy (**4**), 2-Etpy (**5**), py (**6a**), 3-Mepy (**7a**) or 4-Mepy (**8a**), and [8,9-μ-(H)-9-(PPh$_3$)$_2$-8-(L)-*arachno*-9,6-RhSB$_8$H$_8$], where L = py (**6b**), 3-Mepy (**7b**) or 4-Mepy (**8b**). The selectivity of the reactions depended on the nature of the entering Lewis bases, affording the 6,5-isomers, **2**, **3**, **4** and **5** as single products for PPh$_3$, PCy$_3$, 2-Mepy and 2-Etpy; and mixtures of the 6,5-/9,6-regioisomers, **6a**/**6b**, **7a**/**7b** and **8a**/**8b** for py, 3-Mepy and 4-Mepy, respectively. The molecular structures of both regioisomers were characterized by X-ray diffraction analysis for the 6,5-isomers, **3** and **4**, and for the 9,6-isomers, **7b** and **8b**. Variable temperature NMR studies of the reaction between **1** and PPh$_3$ or 2-Mepy demonstrated that at low temperatures there is formation of the 9,6-species that subsequently isomerizes to the 6,5-regioisomer, indicating that for the more sterically hindered Lewis bases, PPh$_3$, 2-Mepy and PCy$_3$, the latter isomer is more stable and accessible through an intramolecular {Rh(PPh$_3$)$_2$} vertex flip. The formation of both isomers with py, 3-Mepy and 4-Mepy indicates that the kinetic and thermodynamic energies of the 6,5 and 9,6 rhodathiaborane–ligand adducts are similar for these Lewis bases. Lewis base bonding to *exo*-polyhedral boron vertices results in a change of the metal coordination from pseudo-octahedral Rh(III) in **1** to pseudo-square planar Rh(I) in the adducts. The chemistry described here highlights the remarkable structural flexibility of these polyhedral boron-containing compounds, their modular architecture and their easy postsynthetic modification.

Introduction

The possibility to alter the properties of metal complexes by ligand change is without doubt an important driving force for the synthesis of new transition element complexes that may find application in, for example, the activation of small unreactive molecules.[1] In particular, the design of molecular catalysts based on non-innocent ligands with potential to cooperate with the metal centre has witnessed an increasing interest.[2] Some of these complexes promote chemical transformations in which the metal acts, for example, as a Lewis acid centre in cooperation with the surrounding ligand that performs as a base.[3] These metal–ligand cooperations are often referred to as bifunctional mechanisms.

Metallaboranes and metallaheteroboranes are polyhedral boron-based clusters that feature M–B bonds, and incorporate in their framework elements from throughout the periodic table.[4–6] In these molecules, the borane/heteroborane moieties act as polyhapto non-innocent ligands.[7] The vertices in these polyhedral compounds are potentially different reactive centres that allow the modular tuning of the polyhapto borane/heteroborane ligand, leading to rapid and simple assembly of a range of complexes from a common precursor.[8] This postsynthetic modification circumvents the inconvenience of multistep ligand syntheses.

In recent years, we have demonstrated the benefits of this modular approach in the synthesis of a significant range of

[a]*Departamento de Química Inorgánica, Instituto de Síntesis Química y Catálisis Homogénea (ISQCH), Universidad de Zaragoza-CSIC, C/Pedro Cerbuna 12, ES-50009 Zaragoza, Spain. E-mail: rmacias@unizar.es; Tel: +34 876 553 798*

[b]*Centro Universitario de la Defensa, Ctra. Huesca s/n, ES-50090 Zaragoza, Spain*

†Electronic supplementary information (ESI) available: The cif files of X-ray structures of **3**, **4**, **7b** and **8b**, atomic coordinates of calculated structures, and kinetic data. CCDC 1032733, 1456598–1456600. For ESI and crystallographic data in CIF or other electronic format see DOI: 10.1039/c6dt00856a

11-vertex polyhedral metallathiaboranes that bear $\{SB_9H_9\}$ moieties acting as polyhapto ligands bound to a transition metal fragment (Scheme 1). Thus, starting from the rhodathiaborane precursor, $[8,8\text{-}(PPh_3)_2\text{-}nido\text{-}8,7\text{-}RhSB_9H_{10}]$, which exhibits a reactive B–H vertex adjacent to the metal, we have been able to prepare a full family of clusters with N-heterocyclic Lewis bases bound to a boron vertex on the thiaborane ligand.[9–11]

This reaction chemistry highlights the redox structural flexibility of these clusters, which can be altered by the linkage of different Lewis bases to the vertices of the cage. In consequence, we have developed a rich organometallic chemistry based on a family of 11-vertex metallathiaboranes. Overall, we have discovered unprecedented stoichiometric cycles that involve structural redox transformations that are promoted by dehydrogenation/hydrogenation processes in which the dihydrogen is heterolytically cleaved on the clusters. Protonation of some of the metallathiaboranes affords cationic clusters that react with dihydrogen much faster than the neutral species, providing the first examples of proton-assisted H_2 activation by polyhedral boron-containing compounds.[11–13]

Cleavage of dihydrogen on the cluster follows a mechanism in which the metal vertex and the thiaborane fragment simultaneously participate in the bond-breaking and -forming processes, resembling, therefore, the above-mentioned metal–ligand bifunctional systems. This feature has been recently studied by performing DFT calculations dealing with the carbene-ligated rhodathiaborane, $[1,1\text{-}(IMe)(PPh_3)\text{-}3\text{-}(py)\text{-}1,2\text{-}RhSB_9H_8]$ (IMe = 1,3-dimethylimidazol-2-ylidene), which undergoes a cluster rearrangement to accommodate the entering H_2 molecule that is subsequently heterolytically cleaved. This mechanism highlights the involvement of the entire rhodathiaborane cluster in the activation process.

In an attempt to find new types of reactivities promoted by metallathiaboranes, we altered the composition of the polyhapto thiaborane ligand by using a smaller nine vertex cluster based on the $\{SB_8H_8\}$ fragment. And, after systematic reactivity studies, we were able to accomplish the high yield synthesis of $[2,2,2\text{-}(H)(PPh_3)_2\text{-}closo\text{-}2,1\text{-}RhSB_8H_8]$ (**1**), providing the opportunity for the development of the reaction chemistry of this 10-vertex hydridorhodathiaborane.[14] Thus, we found that, similarly to the 11-vertex rhodathiaborane above, compound **1** exhibits reactive B–H centers capable of forming *exo*-polyhedral Ph_3P–B bonds that lead to the formation of the rhodathiaborane adduct, $[6,6\text{-}(PPh_3)_2\text{-}9\text{-}(PPh_3)\text{-}arachno\text{-}6,5\text{-}RhSB_8H_9]$ (compound **2**, see Schemes 1 and 2). This reaction reveals an interesting structural redox switchability that combines the $\{RhH(PPh_3)_2\}$ group and the $\{SB_8H_8\}$ polyhapto ligand in **1**, which has yielded new stoichiometric and catalytic cycles driven by dihydrogen and ethylene.[15]

Similar to the 11-vertex rhodathiaborane introduced above, this reactivity opens the door for a postsynthetic modification of the 10-vertex clusters by the systematic change of the *exo*-polyhedral ligands bound to a boron vertex of the $\{SB_8H_8\}$-fragment. We hypothesized that varying the boron-ligated Lewis base could be a powerful way to tune the reactivity of the 10-vertex rhodathiaboranes. We report herein the reactions of

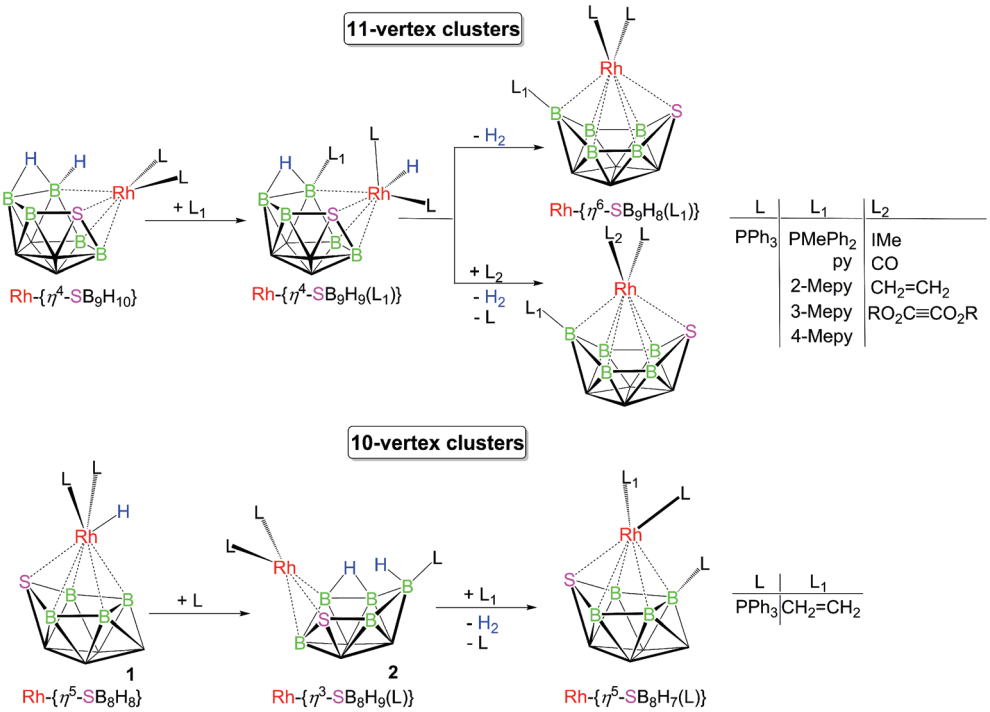

Scheme 1 Postsynthetic modifications of $[8,8\text{-}(PPh_3)_2\text{-}nido\text{-}8,7\text{-}RhSB_9H_{10}]$ and $[2,2,2\text{-}(H)(PPh_3)_2\text{-}closo\text{-}2,1\text{-}RhSB_8H_8]$ (**1**): modular tuning of cluster electronics and sterics. The vertices and the green highlighted boron atoms that do not bear a terminal L substituent represent B–H units.

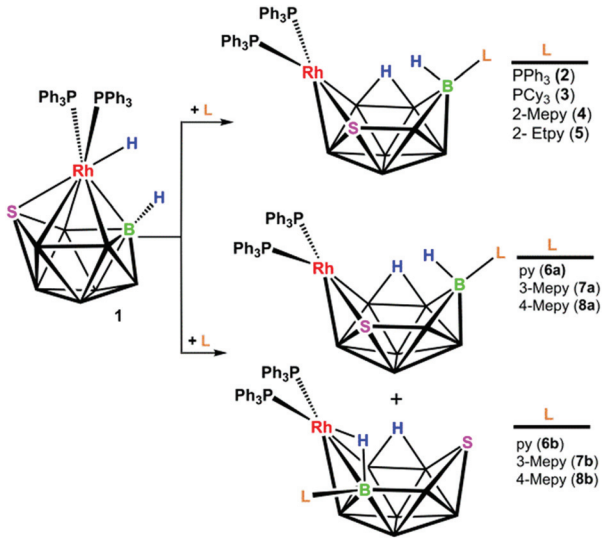

Scheme 2 Reactions of **1** with Lewis bases: synthesis of 10-vertex *arachno*-rhodathiaboranes.

the parent hydridorhodathiaborane **1** with the Lewis bases PCy_3, 2-Mepy, 3-Mepy and 4-Mepy. These reactions have led to the isolation and characterization of a set of new 10-vertex rhodathiaborane–ligand adducts. The compounds were structurally and spectroscopically analyzed in order to understand the metal–thiaborane bonding interaction. A new isomerisation process is also reported, which further illustrates the remarkable chemical and structural flexibility of these types of polyhedral boron-containing compounds.

Results and discussion

Reactions of [2,2,2-(H)$(PPh_3)_2$-*closo*-2,1-$RhSB_8H_8$] (1) with Lewis bases

The treatment of **1** with tris-cyclohexylphosphine (PCy_3), 2-methylpyridine (2-Mepy) and 2-ethylpyridine (3-Etpy) afforded the corresponding polyhedral clusters of the formulation, [6,6-$(PPh_3)_2$-9-(L)-*arachno*-6,5-$RhSB_8H_9$], where L = PCy_3 (**3**), 2-Mepy (**4**) and 2-Etpy (**5**), which are analogues of PPh_3-ligated **2** (Scheme 2). These reactions are selective and give the new 10-vertex rhodathiaboranes in good yields.

In contrast, the use of pyridine (py), 3-methylpyridine (3-Mepy) and 4-methylpyridine (4-Mepy) yielded mixtures of two species: [6,6-$(PPh_3)_2$-9-(L)-*arachno*-6,5-$RhSB_8H_9$] and [8,9-μ-(H)-9-$(PPh_3)_2$-8-(L)-*arachno*-9,6-$RhSB_8H_8$], where L = py (**6a** and **6b**), 3-Mepy (**7a** and **7b**) and 4-Mepy (**8a** and **8b**). Clusters, **6a**, **7a** and **8a** are isostructural counterparts of compounds **2** to **5**; whereas the latter species **6b**, **7b** and **8b** are isomers that exhibit the same basic 10-vertex polyhedral structure (*vide infra*), but with a different metal-to-thiaborane coordination that leads to a change in the positions of the sulphur and the L–B vertex relative to the {$Rh(PPh_3)_2$} group (see Chart 1 and Scheme 2). In other words, both types of compounds are regioisomers.

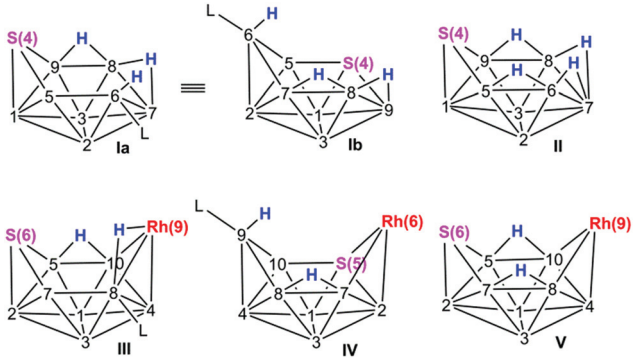

Chart 1

From a descriptive point of view, the formation of the Lewis base–rhodathiaborane adducts can be envisioned as the addition of the metal centre, {$Rh(PPh_3)_2$}, to the neutral 9-vertex thiaborane adducts *exo*-6-L-*arachno*-SB_8H_{10} (Chart 1, schematics **Ia** and **Ib**). In the *arachno*-6,5-isomers the linkage between the metal fragment and the thiaborane cage occurs at the {S(4)B(9)B(8)} vertices of the hexagonal, chair-like face; whereas in the *arachno*-9,6-isomers the metal group is accommodated on the {B(6)B(7)B(8)} section of the same chair-like face of the thiaborane–ligand adducts (Chart 1). This description raises the hypothesis that, alternatively to the procedure described herein, the 10-vertex L-substituted rhodathiaboranes could be synthesized from reaction of *exo*-6-L-*arachno*-SB_8H_{10} with [$RhCl(PPh_3)_3$]: a hypothesis we hope to experimentally test in the future.

In the text, we refer to *arachno* compounds **2–5** and **6a–8a** as 6,5-isomers, and to *arachno* **6b–8b** as 9,6-isomers, where the numerals 6,5 and 9,6 indicate the position of the rhodium and sulphur vertices in the cluster framework (see Chart 1 and Fig. 1 for numbering).

X-Ray diffraction analysis

The molecular structures of **3** and **4** (6,5-isomers), and of **7b** and **8b** (9,6-isomers) were determined by X-ray diffraction analysis. Tables 1 and 2 list selected distances and angles for the new 10-vertex *arachno*-rhodathiaborane together with data for the previously reported PPh_3-ligated derivative, **2**. Fig. 1 shows an ORTEP-type picture for the 2-Mepy- and 3-Mepy-ligated isomers, **4** and **7b**. Both types of isomers exhibit an open, hexagonal boat-shaped face. In the *arachno*-6,5-species, **3** and **4**, there is an {$Rh(PPh_3)_2$} fragment and an {L–B} group, where L = PCy_3 or 2-Mepy, present on opposite sides of the open face and occupying the vertices of connectivity three at positions 9 and 6, respectively. Other structural features of note on the 6,5-isomers, **3** and **4**, also found in previously reported **2**,[14] are the presence of an *endo*-hydrogen atom on the ligand-substituted vertex, L–B(9)–H, and the presence of a bridging hydrogen atom along the B(7)–B(8) edge.

In the *arachno*-9,6-species, **7b** and **8b**, the Lewis base-substituted boron vertex occupies cluster position 8 of connectivity four, adjacent to the metal vertex, on the hexagonal boat-like

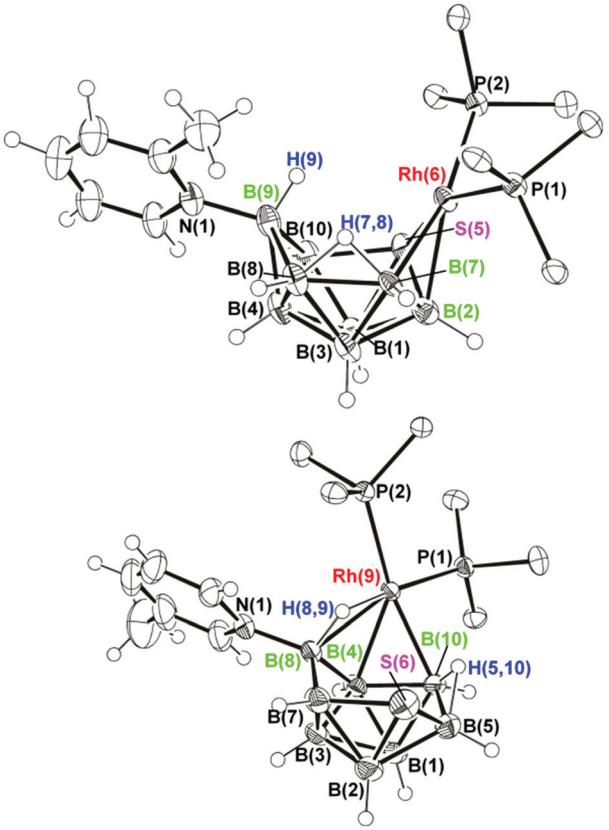

Fig. 1 Solid-state structures for [6,6-$(PPh_3)_2$-9-(2-Mepy)-*arachno*-6,5-$RhSB_8H_9$] (**4**) (top) and [8,9-μ-(H)-9,9-$(PPh_3)_2$-8-(3-Mepy)-*arachno*-9,6-$RhSB_8H_8$] (**7b**) (bottom). Only the *ipso*-carbon atoms on the phenyl groups are included to aid clarity. Ellipsoids are shown at 50% probability levels.

open face. A hydrogen atom bridges the B(8)–Rh(9) edge, and a second hydrogen atom lies along a B–B edge that flanks the positions 6 and 9 of the 10-vertex clusters: the numbering changes from B(7)–B(8) in the 6,5 isomers to B(5)–B(10) in the 9,6 isomers but the edge is formally the same (Fig. 1).

Fig. 2 provides a view that draws attention to the metal–thiaborane linkage in clusters **4** and **7b**, together with, for comparison, the previously reported 10-vertex and 11-vertex rhodathiaboranes, [9,9,9-(CO)(H)$(PPh_3)_2$-*arachno*-9,6-$RhSB_8H_{10}$] (**9**) and [8,8-(PPh_3)-*nido*-$RhSB_9H_{10}$] (**10**).[16] The view of the clusters makes clear that the {$Rh(PPh_3)_2$} group in the isomers **4** and **7b** and the {Rh(CO)(H)$(PPh_3)_2$} moiety in **9** are attached to the corresponding {$SB_8H_9(L)$} and {SB_8H_{10}} fragments, forming a pentagonal pyramid that is highlighted in black solid edges. A similar pyramidal fragment can be recognized in compound **10**, but in this 11-vertex cluster, the {$Rh(PPh_3)_2$} group forms a tetrahapto linkage with the {SB_9H_{10}} fragment that differs from the trihapto interaction found in the three 10-vertex rhodathiaboranes, **4**, **7b** and **9**.

In the three clusters **4**, **7b** and **10** that contain the {$Rh(PPh_3)_2$} fragment, the geometry around the rhodium centre can be described as pseudo-square planar: two bonding vectors are clearly directed toward the phosphine ligands, whereas the other two are more diffusely orientated toward the vertices of the {$SB_8H_9(L)$} fragment that form the trihapto interaction with the metal centre. In this regard, it is reasonable to consider that one of the metal–thiaborane bonding vectors in **4** and **10** points toward the sulfur vertex of the highlighted pyramidal fragment, and toward the 3-Mepy-substituted B(8) vertex in **7b** (see Fig. 2). And the fourth bonding vector could be viewed as directed to the apical vertex of the pentagonal pyramids, B(2) and B(4) in **4** and **7b** respectively, and toward the B(4) vertex in **10**. This description suggests that

Table 1 Selected interatomic distances (Å) for [6,6-$(PPh_3)_2$-9-(PPh_3)-*arachno*-6,5-$RhSB_8H_9$] (**2**), [6,6-$(PPh_3)_2$-9-(PCy_3)-*arachno*-6,5-$RhSB_8H_9$] (**3**) and [6,6-$(PPh_3)_2$-9-(2-Mepy)-*arachno*-6,5-$RhSB_8H_9$] (**4**) with estimated standard uncertainties (s.u.) in parentheses

2[a]		**3**		**4**	
Rh(6)–P(1)	2.726(15)	Rh(6)–P(1)	2.2715(6)	Rh(6)–P(1)	2.2445(9)
Rh(6)–P(2)	2.2872(16)	Rh(6)–P(2)	2.3072(6)	Rh(6)–P(2)	2.2942(9)
Rh(6)–S(5)	2.3364(15)	Rh(6)–S(5)	2.3352(6)	Rh(6)–S(5)	2.3313(9)
Rh(6)–B(2)	2.219(6)	Rh(6)–B(2)	2.239(2)	Rh(6)–B(2)	2.251(4)
Rh(6)–B(7)	2.276(5)	Rh(6)–B(7)	2.262(2)	Rh(6)–B(7)	2.267(3)
S(5)–B(1)	1.992(6)	S(5)–B(1)	1.995(2)	S(5)–B(1)	1.997(4)
S(5)–B(2)	2.035(6)	S(5)–B(2)	2.027(2)	S(5)–B(2)	2.052(4)
S(5)–B(10)	1.916(5)	S(5)–B(10)	1.923(2)	S(5)–B(10)	1.914(4)
P(3)–B(9)	1.929(5)	P(3)–B(9)	1.941(2)	B(9)–N(1)	1.575(5)
B(1)–B(3)	1.741(8)	B(1)–B(3)	1.764(3)	B(1)–B(3)	1.763(6)
B(7)–B(8)	1.858(7)	B(7)–B(8)	1.851(3)	B(7)–B(8)	1.850(5)
B(8)–B(9)[b]	1.888(8)	B(8)–B(9)[b]	1.886(3)	B(8)–B(9)[b]	1.895(6)
B(4)–B(10)[c]	1.715(8)	B(4)–B(9)[c]	1.736(3)	B(4)–B(10)[c]	1.716(6)
B(3)–B(4)	1.778(8)	B(3)–B(4)	1.782(3)	B(3)–B(4)	1.786(6)
S(5)–Rh(6)–B(7)	88.48(13)	S(5)–Rh(6)–B(7)	87.66(6)	S(5)–Rh(6)–B(7)	88.36(9)
P(1)–Rh(6)–P(2)	98.48(5)	P(1)–Rh(6)–P(2)	100.60(2)	P(1)–Rh(6)–P(2)	98.86(3)
P(2)–Rh(6)–B(2)	136.87(14)	P(2)–Rh(6)–B(2)	134.85(6)	P(2)–Rh(6)–B(2)	140.32(11)
P(2)–Rh(6)–B(7)	172.35(13)	P(2)–Rh(6)–B(7)	175.59(6)	P(2)–Rh(6)–B(7)	167.16(10)
P(1)–Rh(6)–S(5)	169.57(5)	P(1)–Rh(6)–S(5)	167.457(19)	P(1)–Rh(6)–S(5)	158.50(3)
P(3)–B(9)–B(4)	114.6(3)	P(3)–B(9)–B(4)	115.31(15)	N(1)–B(9)–B(4)	112.8(3)

[a] Data from ref. 14. [b] Longest B–B distance. [c] Shortest B–B distances.

Table 2 Selected interatomic distances (Å) for [9,8-μ-(H)-9,9-$(PPh_3)_2$-8-(3-Mepy)-*arachno*-9,6-$RhSB_8H_9$] (**7b**) and [9,8-μ-(H)-9,9-$(PPh_3)_2$-8-(4-Mepy)-*arachno*-9,6-$RhSB_8H_8$] (**8b**) with estimated standard uncertainties (s.u.) in parentheses

7b		**8b**	
Rh(9)–P(1)	2.2595(5)	Rh(9)–P(1)	2.2580(6)
Rh(9)–P(2)	2.3191(5)	Rh(9)–P(2)	2.3137(5)
Rh(9)–B(10)	2.2624(17)	Rh(9)–B(10)	2.274(2)
Rh(9)–B(8)	2.3327(17)	Rh(9)–B(8)	2.325(2)
Rh(9)–B(4)	2.2543(17)	Rh(9)–B(4)	2.274(2)
Rh(9)–H(8,9)	1.786(19)	Rh(9)–H(8,9)	1.73(2)
B(8)–H(8,9)	1.193(19)	B(8)–H(8,9)	1.22(2)
S(6)–B(5)	1.932(2)	S(6)–B(5)	1.933(3)
S(6)–B(7)	1.934(2)	S(6)–B(7)	1.935(2)
S(6)–B(2)	1.934(2)	S(6)–B(2)	1.935(2)
B(8)–N(1)	1.572(2)	B(8)–N(1)	1.564(3)
B(1)–B(3)	1.769(3)	B(1)–B(3)	1.759(4)
B(2)–B(3)[a]	1.746(2)	B(2)–B(3)[a]	1.743(3)
B(2)–B(5)[b]	1.939(3)	B(2)–B(5)[b]	1.942(4)
C(2)–C(6)	1.514(3)	C(3)–C(6)	1.501(3)
P(1)–Rh(9)–P(2)	98.97(2)	P(1)–Rh(9)–P(2)	99.912(18)
P(1)–Rh(9)–H(8,9)	168.1(6)	P(1)–Rh(9)–H(8,9)	165.0(8)
P(1)–Rh(9)–B(4)	111.02(5)	P(1)–Rh(9)–B(4)	112.05(6)
P(2)–Rh(9)–B(10)	160.93(5)	P(2)–Rh(9)–B(10)	163.85(6)
B(5)–S(6)–B(7)	98.08(8)	B(5)–S(6)–B(7)	98.43(10)
Rh(9)–B(8)–N(1)	114.28(10)	Rh(9)–B(8)–N(1)	117.42(13)

[a] Shortest B–B distance. [b] Longest B–B distances.

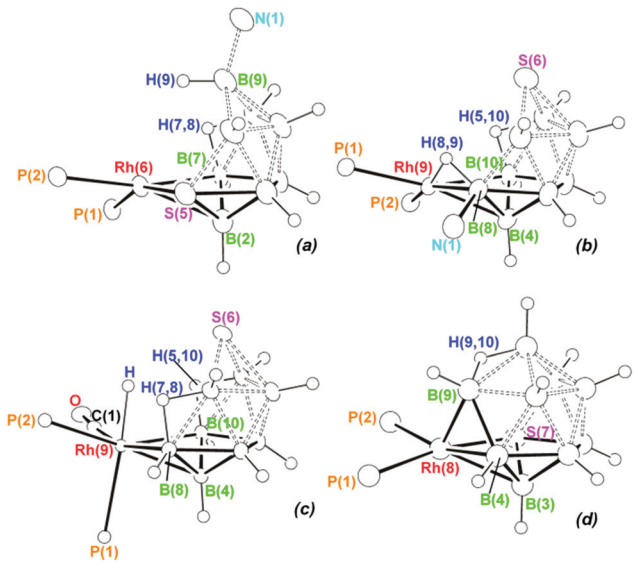

Fig. 2 Details of the rhodium-to-thiaborane linkage in the 10-vertex *arachno*-rhodathiaboranes (a) **4**, (b) **7b** and (c) [9,9,9-(CO)(H)$(PPh_3)_2$-*arachno*-9,6-$RhSB_8H_{10}$] (**9**); and in (d) the 11-vertex rhodathiaborane [8,8-(PPh_3)-*nido*-$RhSB_9H_{10}$] (**10**). Some selected distances and angles of the two latter species are as follows: (c) compound **9**: Rh(9)–P(1) 2.4599(5), Rh(9)–P(2) 2.3711(5), Rh(9)–B(4) 2.241(2), Rh(9)–B(8) 2.288(2), Rh(9)–B(10) 2.302(2), Rh(9)–H 1.55(3), Rh(9)–C(1) 1.9095(19), P(1)–Rh(9)–P(2) 103.33(2), P(1)–Rh(9)–B(10) 170.05(4), P(2)–Rh(8)–B(10) 154.49(5), P(1)–Rh(9)–C(1) 89.02(5), P(2)–Rh(9)–C(1) 95.40(5), B(8)–Rh(9)–C(1) 129.20(7), P(1)–Rh(9)–H 176.1(12); (d) compound **10**: Rh(8)–P(1) 2.2906(11), Rh(8)–P(2) 2.4198(11), Rh(8)–S(7) 2.3769(12), Rh(8)–B(3) 2.243(4), Rh(8)–B(4) 2.236(4), Rh(8)–B(9) 2.145(4), P(1)–Rh(8)–P(2) 98.50(3), P(1)–Rh(8)–S(7) 170.05(4), P(2)–Rh(8)–B(4) 167.05(10).

in **10** there is no interaction between the B(9) vertex and the rhodium centre, and perhaps it would be more realistic to describe the metal–thiaborane interaction as based on a highly distorted square pyramid with the apical position being the B(9) vertex.

It is of interest to point out that the Rh–P distances for the phosphine ligands that lie *trans* to boron vertices [P(2) in Fig. 2] are significantly longer than the phosphines *trans* to the sulfur vertex. This structural trend is a manifestation of the stronger *trans* influence of the cage boron atoms relative to the cage sulfur atoms. A similar situation has been recognized in metallacarboranes, where the cage boron atoms have a larger *trans* influence than the cage carbon atoms.[17] It is also interesting to note that the Rh–P length for the PPh_3 ligand *trans* to the hydride ligand in compound **9** is the longest in this family of polyhedral clusters, demonstrating that the structural *trans* effect of the cage B atoms is not as strong as the effect of a hydride ligand.

From the discussion above, it is clear that the metal-to-thiaborane configuration is directed by the relative *trans* influences of the *exo*-polyhedral ligands with respect to the metal-bound cage atoms. Thus, in compound **9**, the metal hydride, having the choice, avoids lying *trans* to cage boron vertices. The same tendency has been identified in a significant number of hydridometallathiaboranes[9,14,15,18] where the *exo*-polyhedral ligand orientation is mainly controlled by cage S atoms that, in the metal–thiaborane linkage, force the hydride ligands to occupy positions *trans* to the heteroatom: the strong *trans*-influence hydride ligand avoids the cage B atoms that exhibit a stronger structural *trans* effect than the cage sulfur atoms.

An important characteristic of these types of polyhedral boron-containing compounds that we want to highlight in Fig. 2 is their modular architecture, which *a priori* makes possible the interchange of their constituents while maintaining a basic chemical structure. This is an interesting feature since, as pointed out in the Introduction, it permits the modification of the reactivity of a parent cluster simply by changing the units in the "molecular model" (a concept that is well appreciated in the construction of car), saving, therefore, the time that is usually involved in the preparation of different ligands to change the electronic properties of classical coordination complexes. In compounds **4** and **7b**, the sulfur vertex and the Lewis base boron-substituted group, L–B–H, are exchangeable, indicating that both units are isolobal and exhibit a similar bonding interaction within the cluster framework. In addition, from the point of view of the electron counting rules, these two units, S and L–B–H, are also isoelectronic, formally contributing four electrons to the cluster skeletal bonding. It should be noted that the hydrogen atom of the LBH group occupies an *endo*-position in **4**, pointing towards the hexagonal boat-like face; whereas in the 9,6-isomer, **7b**, the hydrogen atom lies bridging along the Rh(9)–B(8) edge.

The modular character of these clusters is further appreciated in the mutual interchangeability of the metal fragments, $\{Rh(PPh_3)_2\}$ and $\{Rh(CO)(H)(PPh_3)_2\}$, in **4** and **9**, respectively. Thus, although these two fragments, according to Wade's

Table 3 ^{11}B and ^{1}H NMR data for [6,6-(PPh$_3$)$_2$-9-(PCy$_3$)-*arachno*-6,5-RhSB$_8$H$_9$] (**3**), [6,6-(PPh$_3$)$_2$-9-(2-Mepy)-*arachno*-6,5-RhSB$_8$H$_9$] (**4**) and [6,6-(PPh$_3$)$_2$-9-(2-Etpy)-*arachno*-6,5-RhSB$_8$H$_9$] (**5**) in CD_2Cl_2 compared to the corresponding DFT/GIAO-calculated ^{11}B-nuclear shielding values [in brackets]

	3		**4**		**5**	
Assig.[a]	$\delta(^{11}B)$ [DFT]	$\delta(^{1}H)$	$\delta(^{11}B)$ [DFT]	$\delta(^{1}H)$	$\delta(^{11}B)$ [DFT]	$\delta(^{1}H)$
B(2)	+15.5 [+19.1]	+3.41	+11.9 [+16.7]	+3.25	+12.3 [+17.5]	+3.59
B(4), B(7)	−5.3 [−1.9, −2.5, −4.3, −5.0]	+2.58, +2.52, +2.23, +2.18	−2.7 [−0.36, −3.1]	+2.67, +2.49	−3.1 [−0.5,−3.3]	+2.68, +2.43
B(8), B(10)			−5.2 [−2.3, −3.6]	+2.55, +2.41	−5.2 [−2.2, −4.05]	+2.58, +2.45
B(9)	−38.9 [−36.6]	−0.45	−17.6 [−18.2]	+1.00	−17.8 [−18.5]	+1.07
B(1)	−26.0 [−24.5]	+1.24	−28.1 [−26.5]	+1.15	−27.7 [−26.8]	+1.56
B(3)	−36.2 [−37.2]	+0.35	−36.9 [−36.9]	+0.34	−36.6 [−35.9]	+0.35
μ-H-(7,8)		−0.6		−0.47		−0.43

[a] Based on ^{1}H–{^{11}B} selective experiments and DFT calculations.

rules,[19] contribute a different number of electrons to the cluster framework [Rh(L)$_2$ one electron *vs.* Rh(H)(L)$_3$ four electrons], they behave as two isolobal fragments that bind the thiaborane framework in a trihapto-fashion: the metal-to-thiaborane interaction is fundamentally the same in both species. Therefore, even though, compounds **4** and **7b** have 10 + 2 skeletal electron pairs (steps) that are typical of 10-vertex *nido*-metallaheteroboranes and **9** has an additional pair (10 + 3) that gives the cage an *arachno*-electron counting, these clusters are nevertheless all conveniently described as 10-vertex *arachno*-species.

Metallaboranes and metallaheteroboranes with 10-vertex *nido*-/*arachno*-structures are well represented in polyhedral boron chemistry.[6,20] The metal fragments that form part of these polyhedral boat-like cages are diverse, and although there are many examples that incorporate the {Pt(L)$_2$} group in the framework,[21,22] 10-vertex *nido*-/*arachno*-rhodadecaboranes and rhodaheterodecaboranes with pseudo-square planar {Rh(L)$_2$} centers in their structures are very uncommon. Previous to this work, the {Rh(PPh$_3$)$_2$} moiety has only been crystallographically characterized as a component of a 10-vertex *nido*-/*arachno*-boat-like cluster in compound **2**.[14]

It should be noted that polyhedral molecules incorporating C_{2v} fragments such as {M(L)$_2$}, where M = Rh, Ir, Pd or Pt, usually do not fulfill the requirements of the electron-counting rules, leading to metallaboranes and metallaheteroboranes that can be one or even two steps short of those formally required by Wade's rules.[23] The discrepancy arises because the metal fragments, {M(L)$_2$}, differ significantly from the isolobal schemes exhibited by the boron vertices and they do not bear additional ligands [*i.e.* Rh(L)$_2$ *vs.* Rh(H)(L)$_3$] that formally contribute the electrons needed to fulfill the counting rules.

Comparative NMR analysis: bonding considerations

All compounds reported in this work were characterized by multielement NMR spectroscopy. The measured data for the PCy$_3$ (**3**), 2-Mepy (**4**) and 2-Etpy (**5**) adducts are gathered in Table 3, and the data for the py (**6a–6b**), 3-Mepy (**7a–7b**) and 4-Mepy (**8a–8b**) counterparts are listed in Table 4. The latter data were measured for samples that contained both isomers, *arachno*-6,5 (**6a–8a**) and *arachno*-9,6 (**6b–8b**). The assignments of the ^{1}H and ^{11}B resonances for all the new ten-vertex rhodathiaboranes were made using ^{1}H–{^{11}B(selective)} experiments and GIAO NMR nuclear shielding predictions on optimized cluster geometries. It should be noted that a reasonable measure of the validity of the calculated structures of these rhodathiaboranes is given by a comparison of the measured ^{11}B NMR chemical shift values and the calculated boron nuclear shielding properties (GIAO approach). The ^{11}B chemical shifts calculated for all the new species reported in this paper reproduce well the experimental trend, and are sufficiently in agreement to support the assignments.

The new Lewis base substituted clusters, reported in this work, exhibit a similar pattern in their ^{11}B NMR spectra with resonances in the interval between δ_B +20 and −40 ppm. The signals corresponding to the cage B(4), B(7), B(8) and B(10) atoms in the *arachno*-6,5 isomers overlap in the region between 0 and −7 ppm, complicating the resolution of the spectra. And the ^{11}B NMR spectra were indirectly resolved by ^{1}H–{^{11}B(selective)} experiments that correlate the broad overlapping signals with four individual B–H terminal proton resonances (Tables 3 and 4). Similarly, the *arachno*-9,6 clusters, **6b–8b** exhibit broad overlapping peaks close to δ_B 0 ppm that correspond to the B(5) and B(7) vertices.

The ^{1}H–{^{11}B} spectra of the ten-vertex rhodathiaboranes show eight proton resonances of a relative intensity one that corresponds to the B–H$_t$ terminal hydrogen atoms, demonstrating that the new Lewis base adducts exhibit C_s point symmetry. It should be noted that the cage bridging hydrogen atoms are diagnostic of the presence of both regioisomers. Thus, in the *arachno*-6,5-isomers, the B(7)–H–B(8) proton resonance appears in the negative region of the spectra close to δ_H −0.4 ppm, whereas for the *arachno*-9,6-isomers, the B(5)–H–B(10) signal appears in the positive region around δ_H +0.1 ppm (Tables 3 and 4). In addition, the *arachno*-9,6-isomers exhibit a very broad doublet around δ_H −5.5 ppm in the ^{1}H–{^{11}B} that broadens significantly in the normal ^{1}H spectrum, demonstrating that the proton couples with cage boron nuclei. Although in the pyridinic 9,6 isomers, **6b–8b**, the $^{2}J_{P,H}$ coupling constant cannot be resolved (in contrast to the PPh$_3$

Table 4 ^{11}B and ^{1}H NMR data for [6,6-$(PPh_3)_2$-9-(py)-*arachno*-6,5-$RhSB_8H_9$] (**6a**), [6,6-$(PPh_3)_2$-9-(3-Mepy)-*arachno*-6,5-$RhSB_8H_9$] (**7a**), [6,6-$(PPh_3)_2$-9-(4-Mepy)-*arachno*-6,5-$RhSB_8H_9$] (**8a**), [9,8-μ-(H)-9,9-$(PPh_3)_2$-8-(py)-*arachno*-9,6-$RhSB_8H_8$] (**6b**), [9,8-μ-(H)-9,9-$(PPh_3)_2$-8-(3-Mepy)-*arachno*-9,6-$RhSB_8H_8$] (**7b**) and [9,8-μ-(H)-9,9-$(PPh_3)_2$-8-(4-Mepy)-*arachno*-9,6-$RhSB_8H_8$] (**8b**) in CD_2Cl_2 compared to the corresponding DFT/GIAO-calculated ^{11}B-nuclear shielding values calculated for the PH_3-models [in brackets]

(a) *arachno-6,5-isomers*

	6a		**7a**		**8a**	
Assig.[a]	δ(^{11}B) [DFT]	δ(^{1}H)	δ(^{11}B) DFT]	δ(^{1}H)	δ(^{11}B) [DFT]	δ(^{1}H)
B(2)	+9.1 [+16.3]	+3.12	+8.7 [+15.8]	+3.10	+9.1 [+16.3]	+3.12
B(4), B(8), B(7), B(10)	−6.3 [−0.6, −0.7, −1.6, −4.8]	+2.66, +2.57, +2.35, +2.28	−6.5 [−0.6, −0.7, −1.6, −4.9]	+2.66, +2.53, +2.34, +2.21	−3.6, −7.0 [−0.7, −0.6, −1.6, −4.8]	+2.54, +2.62, +2.57, +2.27
B(9)	−14.1 [−15.6]	+1.16	−18.5 [−15.7]	+1.16	−15.6 [−15.6]	+1.17
B(1)	−28.9 [−24.6]	+1.14	−28.9 [−24.5]	+1.12	−27.6 [−24.6]	+1.12
B(3)	−37.1 [−35.6]	+0.30	−37.1 [−35.7]	+0.29	−37.4 [−35.6]	+0.29
μ-H-(7,8)		−0.37		−0.38		−0.38

(b) *arachno-9,6-isomers*

6b			**7b**			**8b**		
Assig.[a]	δ(^{11}B) [DFT]	δ(^{1}H)	Assig.[a]	δ(^{11}B) [DFT]	δ(^{1}H)	Assig.[a]	δ(^{11}B) [DFT]	δ(^{1}H)
B(4)	+17.7 [+17.9]	+4.39	B(4)	+17.9 [+19.7]	+4.37	B(4)	+17.8 [+19.7]	+4.38
B(5)		+1.14	B(5)	−0.21 [2.0, −0.8]	+1.17	B(5)	−0.1 [2.0, −0.8]	+1.14,
B(7)	−0.19 [0.0, −0.5]	+2.88	B(7)		+ 2.85	B(7)		+ 2.84
B(3)	−2.6 [−4.7]	+2.76	B(3)	−2.5 [−4.7]	+2.74	B(3)	−2.6 [−4.7]	+2.73
B(2)	−3.6[−7.5]	+2.57	B(2)	−3.5[−8.4]	+2.57	B(2)	−3.6 [−8.4]	+2.56
B(10)	−15.2 [−10.5]	+2.28	B(10)	−15.6 [−13.8]	+2.26	B(10)	−15.6 [−13.8]	+2.27
B(8)	−18.3 [−15.2]	−5.59	B(8)	−18.5 [−18.6]	−5.58	B(8)	−18.3 [−18.6]	−5.59
B(1)	−37.4 [−39.1]	+0.17	B(1)	−37.4 [−37.7]	+0.16	B(1)	−37.4 [−39.1]	+0.14
μ-H-(5,10)		+0.15	μ-H-(5,10)		+0.14	μ-H-(5,10)		+0.15
μ-H-(9,8)		−5.59[b]	μ-H-(9,8)		−5.60[c]	μ-H-(9,8)		−5.66[d]

[a] Based on ^{1}H–{^{11}B} selective experiments and DFT calculations. [b] Very broad d, $^{1}J_{Rh,H}$ = 39 Hz. [c] Very broad d, $^{1}J_{Rh,H}$ = 37 Hz. [d] Very broad d, $^{1}J_{Rh,H}$ = 36 Hz.

ligated 9,6 isomer **2**, which shows a pseudo-quartet at δ_H −8.41, see ref. 14), the proton resonance at the lowest frequency can be assigned with confidence to the Rh(9)–H–B(8) bridging hydrogen atom, being a proof of the presence of the *arachno*-9,6-species *versus* their *arachno*-6,5-isomers.

The basic structure of the nine-vertex non-metallated thiaboranes, schematics **Ia**, **Ib** and **II**, is clearly maintained upon bonding with the rhodium groups and potential information regarding the metal-to-thiaborane bonding interaction in these species may be gained from a comparative study of their ^{11}B NMR spectra. This comparison is represented in Fig. 3. There is an overall shielding in the ^{11}B NMR spectrum of the asymmetric pyridine adduct, *exo*-6-py-4-SB_8H_{10} (bottom trace) with respect to the spectrum of the symmetric non-substituted thiaborane, *arachno*-4-SB_8H_{12} (upper trace). The major changes in the ^{11}B chemical shifts between the two nine-vertex thiaboranes involve the vertices B(2) and B(3) that are *trans* to the B–H–B bridging hydrogen atoms on the hexagonal, chair-like open face and the vertex B(7), antipodal to the sulphur atom. Thus, the signal corresponding to the equivalent B(2) and B(3) nuclei in *arachno*-4-SB_8H_{12} splits into two peaks in the pyridine adduct: the resonance of B(3) shifts 35 ppm toward lower frequencies and that of B(2) moves 8 ppm to higher frequencies. These changes agree with the empirical "μH rule" that

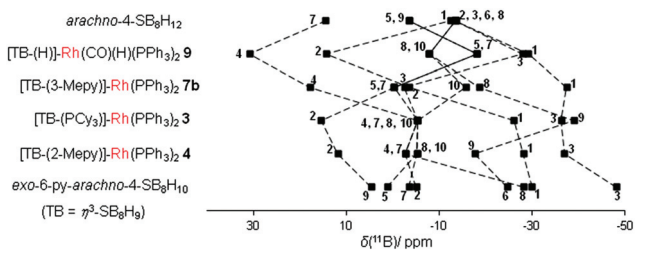

Fig. 3 Representation of the ^{11}B NMR spectra of 9-vertex thiaboranes, *arachno*-4-SB_8H_{12} and *exo*-6-py-*arachno*-4-SB_8H_{10}, [6,6-$(PPh_3)_2$-9-(PCy_3)-*arachno*-6,5-$RhSB_8H_9$] (**3**), [6,6-$(PPh_3)_2$-9-(2-Mepy)-*arachno*-6,5-$RhSB_8H_9$] (**4**), [9,8-μ-(H)-9,9-$(PPh_3)_2$-8-(3-Mepy)-*arachno*-9,6-$RhSB_8H_8$] (**7b**) and [9,9,9-(CO)(H)$(PPh_3)_2$-*arachno*-9,6-$RhSB_8H_{10}$] (**9**). Hatched lines connect equivalent positions. Assignments are made based on DFT-calculations.

assigns a significant lower chemical shift to boron atoms that lie *trans* to B–H–B bridging hydrogen atoms on the open faces of polyhedral boron-containing compounds, compared to boron vertices in the opposite edge of the open-face that do not have μH bridges.[24] Thus, the asymmetry induced by the *exo*-polyhedral substitution of the cage is clearly reflected by the ^{11}B chemical shift of these two signals, B(2) and B(3).

Taking these two nine-vertex thiaboranes as the reference, we can follow the changes that occur in the thiaborane fragment upon the insertion of the metal groups $\{Rh(PPh_3)_2\}$ and $\{Rh(CO)(H)(PPh_3)_2\}$ in order to reach a better understanding of the metal-to-thiaborane bonding interaction. In Fig. 3, we can see that upon insertion of the $\{Rh(CO)(H)(PPh_3)_2\}$ group into the *arachno*-4-SB_8H_{12} cage to form **9**, the resonance for B(1), adjacent to S(4) [B(2) in **9**], undergoes an important shift toward a high frequency, suggesting that the $\{Rh(CO)(H)(PPh_3)_2\}$ fragment exerts a long-range antipodal effect. We can also see a significant frequency shift of the B(7), antipodal to the heteroatom, and a low frequency shift of the resonances, B(2) and B(3), *trans* to the μH bridges.

Similarly, the ^{11}B NMR shielding patterns of the isomeric *arachno*-9,6 and *arachno*-6,5 adducts can be conveniently compared to the parent neutral nine-vertex pyridine-ligated thiaborane, *exo*-6-py-*arachno*-4-SB_8H_{10} (Fig. 3).[25] Overall, there is a small high frequency shift in the ^{11}B NMR spectra of the L-ligated clusters **4**, **3** and **7b**, compared with that of the thiaborane pyridine adduct. In the *arachno*-6,5-isomer, the most significant change corresponds to B(8) in the thiaborane [B(7) in **4**] that shifts ~20 ppm toward a high frequency. Considering that the $\{Rh(PPh_3)_2\}$ fragment subrogates the B(8)–H–B(9) hydrogen atom in the L-ligated thiaboranes (Chart 1, schematics **Ia** and **Ib**), forming a bond with B(7), the mentioned large shift is most likely due to changes in the electronic distribution upon metallation and to deshielding effects of the adjacent PPh_3 ligands.

The main changes in the ^{11}B NMR spectra of the *arachno*-9,6 isomers with respect to the spectrum of *exo*-6-py-*arachno*-4-SB_8H_{10} correspond to the B(2) and B(4) vertices that in the py-ligated adduct are B(1) and B(7), respectively (see Chart 1, schematics **Ia** and **III**). Both signals shift to high frequencies in the rhodathiaborane adducts, perhaps (i) as an enhancement of the antipodal effect of the S(6) vertex on B(4) that may occur upon metallation of the 9-vertex thiaborane–ligand cages, $\{SB_8H_9(L)\}$, at the B(6)–B(7)–B(8) interface, combined with PPh_3 deshielding effects and (ii) as a manifestation of an antipodal effect that the new $\{Rh(PPh_3)_2\}$ vertex may exert on B(2).

It is also worth noting that the resonance of the Lewis base-substituted boron atom suffers a marked shift toward a low frequency when the ligand is PPh_3 or PCy_3 instead of a pyridinic substituent. In this regard, it has been reported that Lewis base–borane adducts such as LBH_3, *arachno*-$[6\text{-L-}B_{10}H_{13}]^-$ and *arachno*-6,9-$L_2B_{10}H_{12}$, where L = NR_3, $NHMe_2$, NH_2Me, PPh_3, PMe_3, *etc.*, exhibit a high frequency shift of 20–30 ppm in the ^{11}B NMR signal of the L-substituted vertex with ammines and pyridine with respect to the values of the phosphine-ligated adducts.[24]

The changes in the ^{11}B NMR pattern of the thiaborane fragments $\{SB_8H_{10}\}$ and $\{SB_8H_9L\}$ upon bonding to the metal fragments $\{Rh(CO)(H)(PPh_3)_2\}$ and $\{Rh(PPh_3)_2\}$, respectively, have been rationalized mainly based on long-range antipodal effects of the metal and the sulphur vertices and on the empirical "μH rule".[24] It is reasonable to assume that the $\{Rh(CO)(H)(PPh_3)_2\}$ fragment in compound **9** acts, to a large extent, as a surrogate of the two μH bridges along the B(6)–B(7) and B(7)–B(8) edges in the parent nine-vertex thiaborane *arachno*-4-SB_8H_{12}.

Similarly, the metal fragment $\{Rh(PPh_3)_2\}$ in the rhodathiaborane–ligand adducts subrogates a μH bridging hydrogen atom along the B(8)–B(9) and the B(7)–B(8) edges (depending on the isomer) of the nine-vertex thiaboranes adducts, *arachno*-L-SB_8H_{10} (schematics **Ia** and **Ib**). The metallathiaborane adducts may, therefore, be regarded as Rh(I) sixteen-electron complexes formed by the interaction of the $\{Rh(PPh_3)_2\}^+$ moiety with the [L-*arachno*-4-SB_8H_9]$^-$ groups acting as trihapto ligands with bidentate character. Since the deprotonation of B–H–B bridging hydrogen atoms in polyhedral boron-containing compounds is a well known reaction,[5,6,14,26] anionic [6-L-*arachno*-4-SB_8H_9]$^-$ can be *a priori* prepared as individual ligands, providing, as commented above, an alternative route to the synthesis of the herein reported ten-vertex metallathiaborane adducts.

Kinetic studies and mechanistic considerations

The reaction between the hydridorhodathiaborane, **1**, and 2-Mepy was studied by ^{1}H NMR spectroscopy, monitoring the decrease of the Rh–H hydride resonance *versus* time. The concentration of 2-Mepy was kept in excess to hold the pseudo-first-order conditions. The values of k_{obs} for different concentrations of 2-picoline are summarized in Table 5, together with the data previously reported by us for the reaction with PPh_3.[14] The analysis of the variation of the concentration of **1** with the time follows a first-order kinetic with respect to this reactant and the plot of k_{obs} *versus* [2-Mepy] reveals a reaction order of one. Therefore, the reaction of **1** with 2-Mepy obeys an overall second-order rate law in agreement with the results found with PPh_3 as the reactant.

In the reaction of the 10-vertex hydridorhodathiaborane, **1**, with PPh_3 to give the *arachno*-adduct, **2**, we detected the formation of an intermediate that, in the ^{1}H–{^{11}B} NMR spectrum, exhibited a pseudo-quartet at δ_H −8.41 ppm, diagnostic of the presence of a Rh–H–B bridging hydrogen atom. This intermediate evolved to give the *arachno*-cluster, **2**, following a zero-order kinetic. Without X-ray diffraction data, we proposed that the intermediate was an *arachno*-6,5-species with a bridging hydrogen atom along the Rh(6)–B(7) edge and the trans-

Table 5 Pseudo-first order constants for the reactions of **1** with PPh_3 and 2-Mepy at 298 K. $[\mathbf{1}]_0$ = 0.004 mol L^{-1}

[PPh_3] (mol L^{-1})	k_{obs} [a] × 10^3 (s^{-1})	[2-Mepy] (mol L^{-1})	k_{obs} [a] × 10^3 (s^{-1})
0.028	1.37	0.024	0.35
0.042	1.97	0.04	0.8
0.047	2.33	0.049	0.9
0.060	2.37	0.061	1.0
0.071	3.87	0.085	1.2
0.079	3.63	0.11	1.6
0.10	5.40	—	—

[a] Values obtained from three measurements.

formation into **2** was described, therefore, as a simple migration of the Rh(6)–H–B(7) bridging hydrogen atom to the B(7)–B(8) edge of the hexagonal boat-like face of the 10-vertex *arachno*-cluster (Chart 1, schematic **IV**).[14]

The reactions reported herein with a range of Lewis bases have revealed unambiguously that there is a formation of two regioisomers: *arachno*-6,5 and *arachno*-9,6. Therefore, it is clear that the intermediate detected at low temperatures in the reaction between **1** and PPh_3 is the *arachno*-9,6-isomer that subsequently undergoes cluster rearrangement to form the *arachno*-6,5-isomer. The PPh_3-ligated *arachno*-9,6-species is sufficiently stable to permit the study of its transformation into the *arachno*-6,5-isomer.

In the case of the reaction with 2-Mepy, the *arachno*-9,6-isomer [9,8-μ-(H)-9,9-$(PPh_3)_2$-8-(2-Mepy)-*arachno*-9,6-$RhSB_8H_8$] was identified as an intermediate in mixtures that contained the starting material, **1** and the 6,5-isomer, **4** as major components. The fast isomerization of the minor intermediate precluded a kinetic study of the *arachno*-9,6 → *arachno*-6,5 isomerization.

The spectroscopic data for the 2-Mepy-ligated 9,6-isomer are consequently limited due to the low concentration of this species and the fact that some signals in the $^{1}H–\{^{11}B\}$ and ^{11}B NMR spectra overlap with those of the major components, **1** and **4**. However, the $^{1}H–\{^{11}B\}$ NMR spectrum shows a broad doublet of doublets at δ_H −6.56 that can be assigned with confidence to the Rh(9)–H(8,9)–B(8) bridging hydrogen atom, being, as mentioned above, diagnostic of the presence of the *arachno*-9,6-species *versus* its *arachno*-6,5-isomer (Fig. S1†). The low intensity doublet of doublets at δ_P +26.7 and +49.3 in the $^{31}P–\{^{1}H\}$ NMR spectrum can also be assigned with confidence to the 2-Mepy-ligated kinetic intermediate (Fig. S3†).

The mechanism of conversion of the 9,6 isomer to the 6,5 isomer may seem to take place through a Rh(9)-vertex transfer (or flip) and a concomitant movement of the B(5)–H–B(10) bridging hydrogen atom to the B(7)–B(8) edge (Scheme 3). Cluster rearrangements by vertex flips have been invoked, for example, to rationalize the fluxional enantiomerization of $[(PMe_2Ph)_2PtS_2B_7H_7]$ and also for the conversion of *nido*-6-iridadecaboranes to *nido*-5-iridadecaboranes.[22,27]

These results have revealed that the 9,6 isomers are the kinetic products that subsequently rearrange to give the 6,5 species. Thus, under typical work-up conditions, the reactions with PPh_3, PCy_3, 2-Mepy and 2-Etpy afford selectively the 6,5 isomers, and it was only during our experiments at low temperatures that we could detect in solution the 9,6 species for the reactions with PPh_3 and 2-Mepy. The selectivity of the reaction is lower for the reactants, py, 3-Mepy and 4-Mepy, which affords mixtures of both isomers. The presence of the 9,6 isomers in higher ratios than the 6,5 isomers suggests that the formers are slightly more stable although it is clear that for the less sterically hindered ligands, py, 3-Mepy and 4-Mepy, the kinetic and thermodynamic stability of both regioisomers is very similar.

DFT calculations on the py-, 2-Mepy- and PPh_3-ligated rhodathiaborane adducts demonstrated that the 9,6 isomers with PPh_3 and 2-Mepy substituents at the boron-8, adjacent to the metal centre, are around 5 kcal mol^{-1} higher in energy than the corresponding 6,5 isomers (Fig. 4); whereas for the py, 3-Mepy and 4-Mepy ligated adducts, **6a**/**6b**, **7a**/**7b** and **8a**/**8b**, the difference in energy between the two isomers is around 1 kcal mol^{-1}. These calculated relative energy differences of the ground states in the set of rhodathiaborane-ligated adducts [6,6-$(PPh_3)_2$-9-(L)-*arachno*-6,5-$RhSB_8H_9$] and [9,9-$(PPh_3)_2$-8-(L)-*arachno*-9,6-$RhSB_8H_9$], where L = py, 2-Mepy, 3-Mepy, 4-Mepy and PPh_3, are small; however, the data support that steric hindrance imposed by the entering Lewis base, which finally bonds to a boron vertex, plays a role in the outcomes of the reactions with **1**.

In other words, the transformation of the *arachno*-9,6-products to give the *arachno*-6,5-regioisomers is driven, to an important degree, by steric interactions between the *exo*-polyhedral boron-bound ligands, L, and the PPh_3 ligands at the metal centre. The kinetic studies reported previously for the reaction of **1** with PPh_3 and herein with 2-Mepy demonstrate a bimolecular process. However, the intimate mechanism of interaction between the *closo*-hydridorhodathiaborane and the incoming Lewis base to form the transition state through which the system evolves to give the rhodathiaborane-ligated

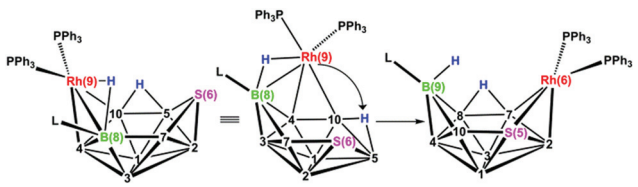

Scheme 3 *Arachno*-9,6 → *arachno*-6,5 isomerization *via* a metal vertex flip.

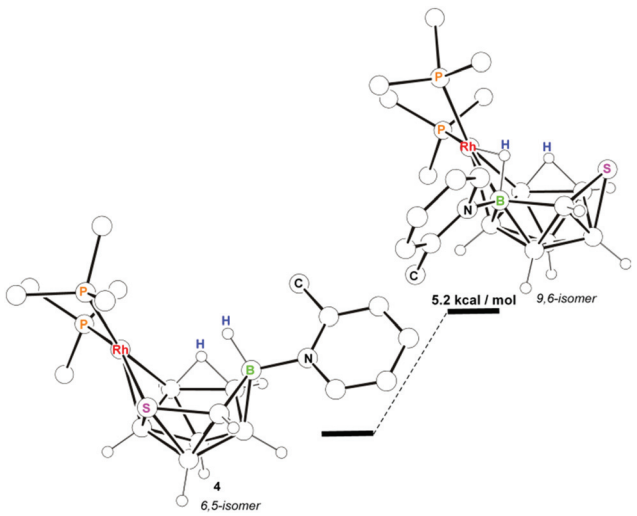

Fig. 4 DFT-calculated energy and structures, computed at the B3LYP/6-31G*/LANL2DZ level for [6,6-$(PPh_3)_2$-9-(2-Mepy)-*arachno*-6,5-$RhSB_8H_9$] (**4**) and its *arachno*-9,6-isomer.

adducts (6,5 and 9,6 regioisomers) is unknown at this time. We can speculate that the entering ligand attacks the *closo*-cluster at the metal centre, an adjacent boron vertex or an Rh–B edge. Regardless of the mechanism, it is important to keep in mind that the hydridorhodathiaborane reagent, **1**, exhibits an inherent stereochemical non-rigidity that facilitates, first the interaction of the Lewis base with the reactive vertices of the 10-vertex *closo*-cage, and second, the reorganization of the system to form a transition state that finally allows the formation of the *arachno*-regioisomers. As demonstrated in other examples, structural flexibility in metallaboranes and metallaheteroboranes is the key feature in the activation of unreactive molecules such as dihydrogen.[12]

In the reactions with PPh_3 and 2-Mepy, it have been demonstrated that the 6,5 isomer is the thermodynamic product that can be formed from the 9,6 isomer; however, we should consider that the more stable 6,5 isomer could be accessible directly from a bimolecular transition state without forming the 9,6 isomer. This idea arises from the perception that the formation of a 9,6 isomer bearing the very bulky PCy_3 ligand is very unlikely and, therefore, it is reasonable to believe that the pathway toward the 6,5 isomer may not require the formation of the 9,6 isomer, and that both isomers may be accessible from a common transition state.

Experimental

General procedures

The reactions were carried out under an argon atmosphere using standard Schlenk-line techniques. Dry solvents were obtained from a Solvent Purification System from Innovative Technology Inc. The thiaborane *arachno*-4-SB_8H_{12},[28] the [PSH][*arachno*-4-SB_8H_{11}] salt and Wilkinson's compound [$RhCl(PPh_3)_3$] were prepared according to the literature methods.[14,29] All other reactants were used as received.

Infrared spectra were recorded on a Perkin-Elmer 100 spectrometer, using a Universal ATR Sampling Accessory. NMR spectra were recorded on Brüker Avance 300 MHz and AV 400 MHz spectrometers, using ^{31}P–{^1H}, ^{11}B, ^{11}B–{^1H}, ^1H, ^1H–{^{11}B} and ^1H–{^{11}B(selective)} techniques. Residual solvent protons were used as the reference (δ, ppm, dichloromethane, +5.32). ^{11}B chemical shifts are quoted relative to [$BF_3(OEt)_2$] and ^{31}P chemical shifts are quoted relative to H_3PO_4. Mass spectra were obtained on a Micro Tof-Q Bruker Daltonics spectrometer. Elemental analyses C/H/N were carried out using a Perkin-Elmer 2400 CHNS/O analyzer.

Compounds **1** and **2** were prepared using optimized procedures that are different from those published by us in ref. 14. The new synthesis of **1** and **2** is reported below.

Solid state structure determinations

Single crystals of [6,6-$(PPh_3)_2$-9-(PCy_3)-*arachno*-6,5-$RhSB_8H_9$] (**3**), [6,6-$(PPh_3)_2$-9-(2-Mepy)-*arachno*-6,5-$RhSB_8H_9$] (**4**), [9,8-μ-(H)-9,9-$(PPh_3)_2$-8-(3-Mepy)-*arachno*-9,6-$RhSB_8H_8$] (**7b**) and [9,8-μ-(H)-9,9-$(PPh_3)_2$-8-(4-Mepy)-*arachno*-9,6-$RhSB_8H_8$] (**8b**), suitable for X-ray diffraction analysis, were grown by slow diffusion of hexane into a dichloromethane solution of the corresponding rhodathiaborane. The diffraction data were collected at 100(2) K on a Bruker APEX DUO diffractometer equipped with an area detector and using graphite monochromatic MoK_α radiation (0.7107073 Å), following standard procedures. The intensities of the diffraction peaks were integrated including Lorentz and polarization effects with the SAINTS-Plus program,[30] and corrected for absorption effects by multiscan methods (SADABS).[31] Refinement was carried out against all F^2 by full-matrix least-squares procedures (SHELXL-97).[32] The structures were refined first with isotropic and later with anisotropic displacement parameters for non-hydrogen atoms. B–H hydrogen atoms were observed in Fourier difference maps and freely refined in the borane fragments; whereas most C–H hydrogen atoms were placed in calculated positions with fixed isotropic thermal parameters. Tables 1 and 2 gather selected distances and angles, and below the reader can find relevant crystallographic data for compounds **3**, **4**, **7b** and **8b**.

Crystal data for 3. $C_{54}H_{72}B_8P_3RhS{\cdot}CH_2Cl_2$; M = 1120.40 g mol^{-1}; orange prism, 0.148 × 0.111 × 0.102 mm^3; triclinic; $P\bar{1}$; a = 9.5067(13) Å, b = 12.2200(17) Å, c = 26.458(4) Å, α = 88.643(2)°, β = 81.179(2)°, γ = 69.276(2)°; Z = 2; V = 2839.2(7) Å^3; D_c = 1.311 g cm^{-3}; μ = 0.552 mm^{-1}; min. and max. absorption correction factors 0.8130 and 0.9516; $2\theta_{max}$ = 58.85°; limiting indices: $-13 \le h \le 12$, $-15 \le k \le 16$, $-36 \le l \le 36$; 31 476 reflections collected, 14 390 unique (R_{int} = 0.0342); number of data/restraints/parameters 14 395/0/927; final GOF = 1.026; R_1 = 0.0358 [$I > 2\sigma(I)$], 0.0458 (all data); wR_2 = 0.0830 [$I > 2\sigma(I)$], 0.0877 (all data). CCDC deposit number 1456598.

Crystal data for 4. $C_{42}H_{46}B_8NP_2RhS{\cdot}CHCl_3$; M = 967.56 g mol^{-1}; red cube, 0.171 × 0.140 × 0.102 mm^3; monoclinic; $P2_1/c$; a = 16.0929(11) Å, b = 10.6606(8) Å, c = 26.1385(18) Å, α = 90°, β = 93.3030(10)°, γ = 90°; Z = 4; V = 4476.9(5) Å^3; D_c = 1.436 g cm^{-3}; μ = 0.712 mm^{-1}; min. and max. absorption correction factors 0.8234 and 0.9422; $2\theta_{max}$ = 58.02°; limiting indices: $-21 \le h \le 20$, $-14 \le k \le 14$, $-35 \le l \le 35$; 73 083 reflections collected, 11 821 unique [R_{int} = 0.0751]; data/restraints/parameters: 11 821/0/671; final GOF = 1.037; R_1 = 0.0466 [$I > 2\sigma(I)$], 0.0951 (all data); wR_2 = 0.1014 [$I > 2\sigma(I)$], 0.1231 (all data). CCDC deposit number 1032733.

Crystal data for 7b. $C_{42}H_{46}B_8NP_2RhS$; M = 848.19 g mol^{-1}; red prism, 0.290 × 0.230 × 0.210 mm^3; monoclinic; $P2_1/n$; a = 12.885(2) Å, b = 20.215(4) Å, c = 16.344(3) Å, α = 90°, β = 101.309(2)°, γ = 90°; Z = 4; V = 4174.7(13) Å^3; D_c = 1.349 g cm^{-3}; μ = 0.568 mm^{-1}; min. and max. absorption correction factors 0.801 and 0.888; 2θ = 54.96°; limiting indices: $-16 \le h \le 15$, $-26 \le k \le 26$, $-21 \le l \le 21$; 81 352 reflections collected, 9573 unique [$R_{(int)}$ = 0.0345]; data/restraints/parameters: 9573/1/669; final GOF = 1.046; R_1 = 0.0238 [$I > 2\sigma(I)$], 0.0273 (all data); wR_2 = 0.0600 [$I > 2\sigma(I)$], 0.0624 (all data). CCDC deposit number 1456599.

Crystal data for 8b. **2**·($C_{42}H_{46}B_8NP_2RhS$)·1/2(CH_2Cl_2); M = 1781.30 g mol^{-1}; orange prism, 0.220 × 0.110 × 0.100 mm^3; triclinic; $P\bar{1}$; a = 11.2617(12) Å, b = 13.1022(14) Å, c = 16.6998(18) Å, α = 79.2790(10)°, β = 75.5540(10)°, γ = 65.0620(10)°;

Z = 1; V = 2154.5(4)) Å^3; D_c = 1.373 g cm^{-3}; μ = 0.614 mm^{-1}; min. and max. absorption correction factors 0.877 and 0.941; 2θ = 57.34; limiting indices: $-13 \leq h \leq 13$, $-15 \leq k \leq 15$, $-27 \leq l \leq 27$; 50 593 reflections collected, 10 360 unique [$R_{(int)}$ = 0.0323], data/restraints/parameters: 10 360/0/557; final GOF = 1.036; R_1 = 0.0317 [$I > 2\sigma(I)$], 0.0396 (all data); wR_2 = 0.0720 [$I > 2\sigma(I)$], 0.0763 (all data). CCDC deposit number 1456600.

Calculations

All calculations were performed using the Gaussian 09 package.[33] Structures were initially optimized using standard methods with the STO-3G* basis-sets for C, B, P, S and H, and with the LANL2DZ basis-set for the rhodium atom. The final optimizations, including frequency analyses to confirm the true minima, were performed using the B3LYP methodology, with the 6-31G* and LANL2DZ basis-sets. The GIAO nuclear shielding calculations were performed on the final optimized geometries, and computed ^{11}B shielding values were related to chemical shifts by comparison with the computed value for B_2H_6, which was taken to be $\delta(^{11}B)$ +16.6 ppm relative to the $BF_3(OEt_2)$ = 0.0 ppm standard.

Synthesis of [2,2,2-(PPh$_3$)$_2$(H)-*closo*-2,1-RhSB$_8$H$_8$] (1). 0.2 g of [PSH][SB$_8$H$_{11}$] (0.6 mmol) was placed in a Schlenk tube under an argon atmosphere, and the salt was dissolved in 18 mL of dry dichloromethane. The tube was immersed in an isopropanol bath at −35 °C, then an equimolar amount of [RhCl(PPh$_3$)$_3$] (0.56 g) was added to the solution and the mixture was stirred at −35 °C. After 15 minutes, the reaction mixture was filtered through silica gel. The filtrate was collected in a Schlenk tube and placed in an isopropanol bath at −15 °C. After low temperature solvent evaporation, addition of hexane gave **1** as a yellow precipitate that was washed with hexane (6 × 10 ml), isolated by filtration and dried in a vacuum. Yield 0.34 g (77%, 0.33 mmol).

Synthesis of [6,6-(PPh$_3$)$_2$-9-(PPh$_3$)-*arachno*-6,5-RhSB$_8$H$_9$] (2). 0.2 g of [PSH][SB$_8$H$_{11}$] (0.6 mmol) was placed under an argon atmosphere in a Schlenk tube and dissolved in 18 mL of dry dichloromethane. 0.56 g of [RhCl(PPh$_3$)$_3$] (0.6 mmol) was added at −35 °C and the solution was stirred for 15 minutes at a low temperature. Then the reaction mixture was filtered through silica gel and the solvent was reduced in volume until 10 mL. The remaining solvent was degassed and then 0.46 g of crystallized PPh_3 (1.18 mmol) was added. The mixture was stirred for 5 hours at room temperature. After solvent evaporation and addition of hexane, compound **2** was isolated as a yellow precipitate. The solid was washed with hexane (6 × 10 ml), filtered and dried in a vacuum. Yield 0.4 g (67%, 0.39 mmol).

Synthesis of [6,6-(PPh$_3$)$_2$-9-(PCy$_3$)-*arachno*-6,5-RhSB$_8$H$_9$] (3). 51 mg (0.07 mmol) of the hydridorhodathiaborane, **1**, was placed in a Schlenk tube, and the system was subjected to dynamic vacuum for 10 minutes. After this time, the Schlenk tube was transferred to a dry box, where 57 mg of PCy_3 (0.2 mmol) was added together with 5 mL of dry and deoxygenated CH_2Cl_2. The reaction mixture was stirred for 6 hours. The dichloromethane solvent was reduced in volume, and hexane was added to afford the precipitation of a yellow solid. This product was washed three times with hexane, and the supernatant was removed with a Pasteur pipette. The remaining product was dried under vacuum for 8 hours to obtain 49 mg of a yellow solid that was characterized as **3** (0.05 mmol, 69%). Table 3 gathers the main ^{11}B–{^{1}H} and ^{1}H–{^{11}B} NMR data for **3** and additional NMR data are given below. IR (ATR): ν_{max}/cm^{-1} 2523 m (BH). ^{1}H NMR (300 MHz; CD_2Cl_2; 298 K): δ 7.42–7.03 (30H, m, P*Ph*$_3$), 2.03–1.28 (33H, m, P*Cy*$_3$). ^{31}P–{^{1}H} NMR (121 MHz; CD_2Cl_2, 298 K): δ +46.6 (1P, dd, $^1J_{P,Rh}$ = 199 Hz, $^2J_{P,P}$ = 35 Hz, PPh_3), +31.9 (1P, dd, $^1J_{P,Rh}$ = 156 Hz, PPh_3), +11.3 (1P, br, B-PCy_3).

Synthesis of [6,6-(PPh$_3$)$_2$-9-(2-Mepy)-*arachno*-6,5-RhSB$_8$H$_9$] (4). A Schlenk tube was loaded with 0.14 g of **1** (0.18 mmol) and evacuated. Then, 10 mL of CH_2Cl_2 was injected under an argon atmosphere. After degassing the solution, 54 μL of degassed 2-methylpyridine (52 mg, 0.55 mmol) was added. The reaction mixture was stirred at room temperature for 7 hours. Then, the solvent was evaporated under reduced pressure. The addition of hexane gave a mustard coloured precipitate. The product was washed with hexane (5 × 10 ml) and isolated by filtration with a cannula. After drying under vacuum, 0.13 g of compound **3** was obtained (83% yield). Table 3 lists the main ^{11}B–{^{1}H} and ^{1}H–{^{11}B} NMR data for **4** and additional NMR data are given below. Anal. Calcd for $B_8C_{42}H_{46}NP_2RhS\cdot(CH_2Cl_2)$: C, 55.35; H, 5.47; N, 1.65; S, 3.78. Found: C, 54.02; H, 5.20; N, 1.68; S, 3.25. IR (ATR): ν_{max}/cm^{-1} 2533 m (BH). ^{1}H–{^{11}B} NMR (300 MHz, CD_2Cl_2, 298 K): δ +8.76 (1H, d, $^3J_{H,H}$ = 5.9 Hz, H_o-NC_6H_7), +7.88 (1H, t, $^3J_{H,H}$ = 8.6 Hz, H_p-NC_6H_7), +7.66 (1H, m, H_m-NC_6H_7), +7.54 (1H, m, H_m-NC_6H_7) +7.42 to +6.83 (30H, m, 2 PPh_3), +2.83 (3H, s, CH_3-NC_6H_7). ^{31}P–{^{1}H} NMR (121 MHz; CD_2Cl_2, 298 K): δ +47.1 (1P, dd, $^1J_{P,Rh}$ = 120 Hz, $^2J_{P,P}$ = 33 Hz, PPh_3), +32.1 (1P, dd, $^1J_{P,Rh}$ = 151 Hz, $^2J_{P,P}$ = 36 Hz, PPh_3). HRMS (μ-TOF): *m*/*z* calcd maximum for [M − H]$^+$ $B_8C_{42}H_{45}NP_2RhS$, 847.2603; obsd, 847.2590. The envelope for the measured masses for **4** matches that calculated from the isotopic abundances of the constituent elements.

In NMR studies at low temperatures, we detected the 9,6-isomer, [9,8-μ-(H)-9,9-(PPh$_3$)$_2$-8-(2-Mepy)-*arachno*-9,6-RhSB$_8$H$_8$] as a minor intermediate that undergoes fast transformation to give **4**. The following are the NMR data that we could collect from those studies in samples that contained **1** and **4** as major products.

NMR data for the *arachno*-9,6-isomer: ^{1}H (500 MHz; CD_2Cl_2; 283 K): δ +8.10 (2H, d, $^3J_{H,H}$ = 5.6 Hz, H_o-4-CH_3-NC_5H_5), +7.48 (2H, m, H_m-4-CH_3-NC_5H_5), +7.41 to +6.92 (30H, m, 2P*Ph*$_3$), +3.46 (s, BH), +3.07 (s, BH), +1.70 (s, BH), +1.54 (s, BH), +0.82 (s, BH), −6.56 [dd, $^1J_{Rh,H}$ = 44.6 Hz, $^2J_{P,H}$ = 16.4 Hz, Rh(9)–H(8,9)–B(8)]. ^{31}P–{^{1}H} (121 MHz; CD_2Cl_2, 283 K): δ +49.3 (1P, dd, $^1J_{P,Rh}$ = 179 Hz, $^2J_{P,P}$ = 43.8 Hz, PPh_3), +26.7 (1P, dd, $^1J_{P,Rh}$ = 149 Hz, $^2J_{P,P}$ = 43.8 Hz, PPh_3). ^{11}B–{^{1}H} (500 MHz; CD_2Cl_2; 283 K): δ −41.2 (s, $^1J_{H,B}$ = 130 Hz, BH), this is the only signal in the ^{11}B–{^{1}H} NMR spectrum that we could safely assign to the 9,6-isomer: the other peaks are hidden by the high intensity

peaks of the major components in the sample, compounds **1** and **4**.

Synthesis of [6,6-(PPh$_3$)$_2$-9-(2-Etpy)-*arachno*-6,5-RhSB$_8$H$_9$] (5). The procedure described above for 2-picoline was followed. In this case, the reaction was carried out with 100 mg (0.13 mmol) of **1** and 44 μL of 2-ethylpyridine (42 mg, 0.4 mmol). After 14 hours of stirring under an atmosphere of argon, 86 mg of a brown-yellow solid was isolated and characterized as compound **5** (0.10 mmol, 77%). Table 3 gathers the main ^{11}B–{^{1}H} and ^{1}H–{^{11}B} NMR data for **5** and additional spectroscopic data are as follows. IR (ATR): ν_{max}/cm^{-1} 2521 m (BH). ^{1}H NMR (300 MHz; CD_2Cl_2, 298 K): δ +8.81 (1H, d, $^3J_{H,H}$ = 5.9 Hz, H_o-NC$_7$H$_9$), +7.94 (1H, t, $^3J_{H,H}$ = 7.4 Hz, H_p-NC$_7$H$_9$), +7.66 (1H, m, H_m-NC$_7$H$_9$), +7.54 (1H, m, H_m-NC$_7$H$_9$), +7.51 to +6.83 (30H, m, 2P*Ph*$_3$), +3.40 (2H, m, CH$_3$*CH*$_2$-NC$_5$H$_4$), +1.44 (3H, t, *CH*$_3$CH$_2$-NC$_5$H$_4$). ^{31}P–{^{1}H} NMR (121 MHz; CD_2Cl_2, 298 K): δ +47.3 (1P, dd, $^1J_{P,Rh}$ = 200 Hz, $^2J_{P,P}$ = 35 Hz, P*Ph*$_3$), +32.7 (1P, dd, $^1J_{P,Rh}$ = 158 Hz, PPh$_3$). LRMS (MALDI): *m*/*z* calcd maximum for B$_8$C$_{25}$H$_{33}$NPRhS, [M − 2H − (PPh$_3$)]$^+$, 598.2; obsd, 598.3. The envelope for the measured masses for the indicated ion matches that calculated from the isotopic abundances of its constituent elements.

Synthesis of [6,6-(PPh$_3$)$_2$-9-(py)-*arachno*-6,5-RhSB$_8$H$_9$] (6a) and [9,8-μ-(H)-9,9-(PPh$_3$)$_2$-8-(py)-*arachno*-9,6-RhSB$_8$H$_8$] (6b). Following the procedure as above, 104 mg of **1** (0.14 mmol) was treated with 33 μL of pyridine and 6 mL of dry dichloromethane. After two hours of stirring, part of the solvent was evaporated away to favour the precipitation of the product upon addition of hexane; the resulting solid was washed three times with hexane to finally isolate 85 mg of a reddish solid that was characterized as a mixture of the two isomers, **6a** and **6b**, in a 1 : 2 ratio, respectively (0.1 mmol, 75%). IR (ATR): ν_{max}/cm^{-1} 2543–2486 m (BH). LRMS (MALDI$^+$/DIT): *m*/*z* calcd maximum for C$_{23}$H$_{28}$B$_8$NPRhS, [M − (PPh$_3$) − 2(H)]$^+$, 570.9; obsd, 570.2. The envelope for the measured masses for the indicated ion matches that calculated from the isotopic abundances of its constituent elements. Table 4 lists the main ^{11}B–{^{1}H} and ^{1}H–{^{11}B} NMR data for both isomers and additional data are as follows:

8a: ^{1}H NMR (300 MHz; CD_2Cl_2, 298 K): δ +8.51 (2H, d, $^3J_{H,H}$ = 6.1 Hz, H_o-NC$_5$H$_5$), +7.98 (1H, t, $^3J_{H,H}$ = 8.2 Hz, H_p-NC$_5$H$_5$), +7.41 to +7.04 (m, 30H, 2PPh$_3$). ^{31}P–{^{1}H} NMR (121 MHz; CD_2Cl_2, 298 K): δ +47.6 (1P, dd, $^1J_{P,Rh}$ = 200 Hz, $^2J_{P,P}$ = 34 Hz, PPh$_3$), +32.1 (1P, dd, $^1J_{P,Rh}$ = 158 Hz, PPh$_3$).

8b: ^{1}H NMR (300 MHz; CD_2Cl_2, 298 K): δ +8.31 (2H, d, $^3J_{H,H}$ = 5.7 Hz, H_o-NC$_5$H$_5$), +7.74 (1H, t, $^3J_{H,H}$ = 8.4 Hz, H_p-NC$_5$H$_5$), +7.50 (2H, t, $^3J_{H,H}$ = 6.7 Hz, H_m-NC$_5$H$_5$), +7.41 to 7.04 (m, 30H, 2P*Ph*$_3$). ^{31}P–{^{1}H} NMR (121 MHz; CD_2Cl_2, 298 K): δ +44.6 (1P, dd, $^1J_{P,Rh}$ = 176 Hz, $^2J_{P,P}$ = 39 Hz, PPh$_3$), +28.3 (1P, dd, $^1J_{P,Rh}$ = 152 Hz, PPh$_3$).

Synthesis of [6,6-(PPh$_3$)$_2$-9-(3-Mepy)-*arachno*-6,5-RhSB$_8$H$_9$] (7a) and [9,8-μ-(H)-9,9-(PPh$_3$)$_2$-8-(3-Mepy)-*arachno*-9,6-RhSB$_8$H$_8$] (7b). 72 mg of **1** (0.095 mmol) were treated, following the procedures described above, with 28 μL (0.28 mmol) of 3-methylpyridine, freshly distilled and deaerated. After two hours of stirring, and following the work-up as in the preparations above, 57 mg of a brown-red solid were isolated and characterized as the isomer mixture, **7a** and **7b**, in a 0.35 : 1 ratio (0.067 mmol, 71%). IR (ATR): ν_{max}/cm^{-1} 2542–2487 m (BH). LRMS (MALDI$^+$/DIT): *m*/*z* calcd maximum for C$_{24}$H$_{29}$B$_8$NPRhS, [M − (PPh$_3$) − 2(H)]$^+$, 584.2; obsd, 584.2. The envelope for the measured masses for the indicated ion matches that calculated from the isotopic abundances of its constituent elements. Table 4 lists the main ^{11}B–{^{1}H} and ^{1}H–{^{11}B} NMR data for both isomers and additional data are as follows:

7a: ^{1}H NMR (300 MHz; CD_2Cl_2, 298 K): δ +8.38 (1H, d, $^3J_{H,H}$ = 5.9 Hz, H_o-CH$_3$-NC$_5$H$_5$), +7.80 (1H, t, $^3J_{H,H}$ = 8.1 Hz, H_p-CH$_3$-NC$_5$H$_5$), +7.70 (2H, m, H_m-3-CH$_3$-NC$_5$H$_5$), +7.46 to 7.11 (30H, m, 2P*Ph*$_3$), +2.47 (3H, s, 3-C*H*$_3$-NC$_5$H$_5$). ^{31}P–{^{1}H} NMR (121 MHz; CD_2Cl_2, 298 K): δ +47.9 (1P, dd, $^1J_{P,Rh}$ = 200 Hz, $^2J_{P,P}$ = 36 Hz, PPh$_3$), +32.3 (1P, dd, $^1J_{P,Rh}$ = 159 Hz, PPh$_3$).

7b: ^{1}H NMR (300 MHz; CD_2Cl_2, 298 K): δ +8.54 (1H, d, $^3J_{H,H}$ = 6.4 Hz, H_o-3-CH$_3$-NC$_5$H$_5$), +7.59 (1H, d, $^3J_{H,H}$ = 8.1 Hz, H_p-3-CH$_3$-NC$_5$H$_5$), +7.52 (2H, m, H_m-3-CH$_3$-NC$_5$H$_5$), +7.46 to 7.11 (30H, m, 2P*Ph*$_3$), +2.17 (3H, s, 3-*CH*$_3$-NC$_5$H$_5$). ^{31}P–{^{1}H} NMR (121 MHz; CD_2Cl_2, 298 K): δ +44.2 (1P, dd, $^1J_{P,Rh}$ = 176 Hz, $^2J_{P,P}$ = 39 Hz, PPh$_3$), +27.9 (1P, dd, $^1J_{P,Rh}$ = 153 Hz, PPh$_3$).

Synthesis of [6,6-(PPh$_3$)$_2$-9-(4-Mepy)-*arachno*-6,5-RhSB$_8$H$_9$] (8a) and [9,8-μ-(H)-9,9-(PPh$_3$)$_2$-8-(4-Mepy)-*arachno*-9,6-RhSB$_8$H$_8$] (8b). 100 mg of **1** (0.135 mmol) and 39 μL (0.4 mmol) of 4-methylpyridine were stirred for two hours in 5 mL of dry dichloromethane, under an atmosphere of argon. The solvent was reduced in volume to initiate the precipitation of the product, which was washed three times with hexane. The reddish solid was dried under vacuum for 12 hours to give 80 mg (0.094 mmol, 70%) of a mixture of isomers, **8a** and **8b**, in a 0.3 : 1 ratio. IR (ATR): ν_{max}/cm^{-1} 2542–2487 m (BH). LRMS (MALDI$^+$/DIT): *m*/*z* calcd maximum for C$_{24}$H$_{29}$B$_8$NPRhS [M − (PPh$_3$) − 2(H)]$^+$, 584.2; obsd, 584.3. The envelope for the measured masses for the indicated ion matches that calculated from the isotopic abundances of its constituent elements. Table 4 lists the main ^{11}B–{^{1}H} and ^{1}H–{^{11}B} NMR data for both isomers and additional data are as follows:

8a: ^{1}H NMR (300 MHz; CD_2Cl_2; 298 K): δ +8.10 (2H, d, $^3J_{H,H}$ = 5.6 Hz, H_o-4-CH$_3$-NC$_5$H$_5$), +7.48 (2H, m, H_m-4-CH$_3$-NC$_5$H$_5$), +7.41 to +6.92 (30H, m, 2P*Ph*$_3$), 2.48 (3H, s, 4-C*H*$_3$-NC$_5$H$_5$). ^{31}P–{^{1}H} NMR (121 MHz; CD_2Cl_2, 298 K): δ +47.5 (1P, dd, $^1J_{P,Rh}$ = 201 Hz, $^2J_{P,P}$ = 34 Hz, PPh$_3$), +32.1 (1P, dd, $^1J_{P,Rh}$ = 159 Hz, PPh$_3$).

8b: ^{1}H NMR (300 MHz; CD_2Cl_2, 298 K): δ +8.31 (2H, d, $^3J_{H,H}$ = 6.3 Hz, H_o-4-CH$_3$-NC$_5$H$_5$), +7.66 (2H, m, H_m-4-CH$_3$-NC$_5$H$_5$), +7.41 to +6.92 (30H, m, 2P*Ph*$_3$), +2.33 (3H, s, 4-C*H*$_3$-NC$_5$H$_5$). ^{31}P–{^{1}H} NMR (121 MHz; CD_2Cl_2, 298 K): δ +44.5 (1P, dd, $^1J_{P,Rh}$ = 175 Hz, $^2J_{P,P}$ = 39 Hz, PPh$_3$), +28.0 (1P, dd, $^1J_{P,Rh}$ = 152 Hz, PPh$_3$).

Conclusions

The hydridorhodathiaborane, **1**, which exhibits a *closo* structure based on a 10-vertex bicapped square antiprism,

reacts readily with Lewis bases, L, to give a new set of rhodathiaborane–ligand adducts [6,6-$(PPh_3)_2$-9-(L)-6,5-$RhSB_8H_9$] and [8,9-μ-(H)-9-$(PPh_3)_2$-8-(L)-9,6-$RhSB_8H_8$]. These are regioisomers that exhibit a 10-vertex *arachno* structure based on a boat-like polyhedron. In these reactions, the entering ligand attaches to a boron vertex triggering *closo* → *arachno* redox structural responses that result from the increase in the number of the skeletal electron bonding pairs in **1**. This remarkable structural flexibility implies hapticity changes in the metal-to-thiaborane interaction from η^5 to η^3 with the $\{\eta^n\text{-}SB_8H_9(L)\}$ fragments behaving as 'hydride stores'.[34] The NMR spectroscopic data and DFT-calculations support the view that the steric nature of the entering Lewis base plays an important role in the relative kinetic and thermodynamic stability of the isomeric adducts. These stabilities are similar between the 6,5- and 9,6-isomers that bear the less hindered ligands, py, 3-Mepy and 4-Mepy, leading, therefore, to lower selectivity in the reactions with **1**; whereas with the more sterically hindered Lewis bases, PPh_3, PCy_3 and 2-Mepy the energy differences between the regioisomers are larger thus favouring the formation of the 6,5-species in which the entering ligand binds to the B(9) vertex, far from the metal centre. In the reactions with PPh_3 and 2-Mepy at low temperatures, there is a formation of the 9,6 isomer in which the entering Lewis base binds to the B(8) vertex adjacent to the metal centre. At higher temperatures, this regioisomer isomerizes to give the 6,5 species. The isomerization mechanism can be viewed as a flip of the $\{Rh(PPh_3)\}$ vertex on the hexagonal, chair-like face of the $\{SB_8H_9(L)\}$ fragment, resulting in a different metal-to-thiaborane linkage. From a metal point of view, these *arachno*-clusters can be regarded as Rh(I) sixteen-electron complexes formed by the interaction of the $\{Rh(PPh_3)_2\}^+$ moiety with the thiaborane adducts, $[SB_8H_9(L)]^-$, acting as trihapto ligands with bidentate character. Overall, the results described herein emphasize the modular architecture of these polyhedral boron-containing compounds, which makes possible the interchange of their chemical constituents whilst maintaining the basic structure of a 10-vertex boat-like cluster. The redox structural response of **1** to different Lewis bases allows the postsynthetic modification of the 10-vertex model **2**, highlighting the modularity of this system that yields many opportunities to tune the chemical properties of the clusters.

Acknowledgements

We acknowledge the Spanish Ministry of Science and Innovation (CTQ2012-32095, CTQ2009-10132, CONSOLIDER INGENIO, CSD2009-00050, MULTICAT and CSD2006-0015, Crystallization Factory) for support of this work. S. L. thanks the Spanish Ministry of Science and Innovation for a predoctoral scholarship. We acknowledge the helpful comments of Dr J. Bould.

References

1 (*a*) L. A. Berben and J. B. Love, *Chem. Commun.*, 2014, **50**, 7221–7222; (*b*) N. Lehnert and J. C. Peters, *Inorg. Chem.*, 2015, **54**, 9229–9233; (*c*) F. Meyer and W. B. Tolman, *Inorg. Chem.*, 2015, **54**, 5039–5039; (*d*) M. Y. Darensbourg and A. Llobet, *Inorg. Chem.*, 2016, **55**, 371–377.

2 (*a*) J. I. van der Vlugt and J. N. H. Reek, *Angew. Chem., Int. Ed.*, 2009, **48**, 8832–8846; (*b*) C. Gunanathan and D. Milstein, *Acc. Chem. Res.*, 2011, **44**, 588–602; (*c*) M. E. van der Boom and D. Milstein, *Chem. Rev.*, 2003, **103**, 1759–1792; (*d*) M. Albrecht and M. M. Lindner, *Dalton Trans.*, 2011, **40**, 8733–8744.

3 (*a*) R. Noyori, M. Yamakawa and S. Hashiguchi, *J. Org. Chem.*, 2001, **66**, 7931–7944; (*b*) H. Grützmacher, *Angew. Chem., Int. Ed.*, 2008, **47**, 1814–1818; (*c*) Bifunctional Molecular Catalysis, in *Topics in Organometallic Chemistry*, ed. T. Ikariya and M. Shibasaki, Springer, Berlin, Heidelberg, 2011, vol. 37; (*d*) S. Hasegawa, K. Itoh and Y. Ishii, in *Organotransition-Metal Chemistry*, ed. Y. Ishii and M. Tsutsui, Springer US, Boston, MA, 1975, pp. 25–36; (*e*) S. Kuwata and T. Ikariya, *Chem. Commun.*, 2014, **50**, 14290–14300; (*f*) R. H. Morris, *Acc. Chem. Res.*, 2015, **48**, 1494–1502; (*g*) L. A. Berben, B. de Bruin and A. F. Heyduk, *Chem. Commun.*, 2015, **51**, 1553–1554.

4 (*a*) A. S. Weller, in *Comprehensive Organometallic Chemistry III*, ed. R. H. Crabtree and D. M. P. Mingos, Elsevier, Oxford, 2007, vol. 3, pp. 133–174; (*b*) N. S. Hosmane and J. A. Maguire, in *Comprehensive Organometallic Chemistry III*, ed. D. M. P. M. H. Crabtree, Elsevier, Oxford, 2007, pp. 175–264.

5 (*a*) J. D. Kennedy, in *Prog. Inorg. Chem.*, 1984, vol. 32, pp. 519–679; (*b*) L. Wesemann, in *Comprehensive Organometallic Chemistry*, ed. D. M. P. Mingos and R. H. Crabtree, Elsevier, Oxford, 2007, vol. 3, pp. 113–131.

6 J. D. Kennedy, in *Prog. Inorg. Chem.*, 1986, vol. 34, pp. 211–434.

7 N. N. Greenwood, *Coord. Chem. Rev.*, 2002, **226**, 61–69.

8 (*a*) C. J. Jones, J. N. Francis and M. F. Hawthorne, *J. Am. Chem. Soc.*, 1973, **95**, 7633–7643; R. Macías, T. P. Fehlner and A. M. Beatty, *Angew. Chem., Int. Ed.*, 2002, **41**, 3860–3862; (*b*) R. Macías, T. P. Fehlner and A. M. Beatty, *Organometallics*, 2004, **23**, 2124–2136; (*c*) R. Macías, T. P. Fehlner, A. M. Beatty and B. Noll, *Organometallics*, 2004, **23**, 5994–6001.

9 (*a*) B. Calvo, B. Roy, R. Macías, M. J. Artigas, F. J. Lahoz and L. A. Oro, *Inorg. Chem.*, 2014, **53**, 12428–12436; (*b*) A. Álvarez, B. Calvo, R. Macías, F. J. Lahoz and L. A. Oro, *Organometallics*, 2014, **33**, 3137–3153; (*c*) B. Calvo, A. Álvarez, R. Macías, P. García-Orduña, F. J. Lahoz and L. A. Oro, *Organometallics*, 2012, **31**, 2986–2995; (*d*) J. Bould, C. Cunchillos, F. J. Lahoz, L. A. Oro, J. D. Kennedy and R. Macías, *Inorg. Chem.*, 2010, **49**, 7353–7361.

10 (*a*) B. Calvo, M. Keß, R. Macías, R. Sancho, F. J. Lahoz and L. A. Oro, *J. Coord. Chem.*, 2014, **67**, 4016–4027;

(*b*) A. C. Mateo, B. Calvo, R. Macías, M. J. Artigas, F. J. Lahoz and L. A. Oro, *Dalton Trans.*, 2015, **44**, 9004–9013.

11 (*a*) Á. Álvarez, R. Macías, J. Bould, C. Cunchillos, F. J. Lahoz and L. A. Oro, *Chem. – Eur. J.*, 2009, **15**, 5428–5431; (*b*) Á. Álvarez, R. Macías, M. J. Fabra, F. J. Lahoz and L. A. Oro, *J. Am. Chem. Soc.*, 2008, **130**, 2148–2149; (*c*) Á. Álvarez, R. Macías, J. Bould, M. J. Fabra, F. J. Lahoz and L. A. Oro, *J. Am. Chem. Soc.*, 2008, **130**, 11455–11466.

12 B. Calvo, R. Macías, V. Polo, M. J. Artigas, F. J. Lahoz and L. A. Oro, *Chem. Commun.*, 2013, **49**, 9863–9865.

13 B. Calvo, R. Macías, M. J. Artigas, F. J. Lahoz and L. A. Oro, *Chem. – Eur. J.*, 2013, **19**, 3905–3912.

14 S. Luaces, J. Bould, R. Macías, R. Sancho, F. J. Lahoz and L. A. Oro, *Dalton Trans.*, 2012, **41**, 11627–11634.

15 S. Luaces, R. Macías, M. J. Artigas, F. J. Lahoz and L. A. Oro, *Dalton Trans.*, 2015, **44**, 5041–5044.

16 (*a*) S. Luaces, J. Bould, R. Macías, R. Sancho, P. García-Orduña, F. J. Lahoz and L. A. Oro, *J. Organomet. Chem.*, 2012, **721–722**, 23–30; (*b*) G. Ferguson, M. C. Jennings, A. J. Lough, S. Coughlan, T. R. Spalding, J. D. Kennedy, X. L. R. Fontaine and B. Štíbr, *J. Chem. Soc., Chem. Commun.*, 1990, 891–894.

17 A. McAnaw, G. Scott, L. Elrick, G. M. Rosair and A. J. Welch, *Dalton Trans.*, 2013, **42**, 645–664.

18 (*a*) R. Macías, J. Holub, J. D. Kennedy, B. Štíbr and M. Thornton-Pett, *J. Chem. Soc., Chem. Commun.*, 1994, 2265–2266; (*b*) K. Nestor, J. D. Kennedy, M. Thornton-Pett, J. Holub and B. Štíbr, *Inorg. Chem.*, 1992, **31**, 3339–3341; (*c*) J. Bould, N. P. Rath and L. Barton, *Organometallics*, 1996, **15**, 4916–4929.

19 (*a*) K. Wade, *Inorg. Nucl. Chem. Lett.*, 1972, **8**, 563–566; (*b*) K. Wade, *Adv. Inorg. Chem. Radiochem.*, 1976, **18**, 1–66.

20 (*a*) P. Ma, R. Littger, T. M. Smith Pellizzeri, J. Zubieta and J. T. Spencer, *Polyhedron*, 2016, **109**, 129–137; (*b*) P. Ma, T. M. Smith, J. Zubieta and J. T. Spencer, *Inorg. Chem. Commun.*, 2014, **46**, 223–225; (*c*) D. K. Roy, R. S. Anju, B. Varghese and S. Ghosh, *Organometallics*, 2013, **32**, 1964–1970; (*d*) D. K. Roy, S. K. Bose, R. S. Anju, V. Ramkumar and S. Ghosh, *Inorg. Chem.*, 2012, **51**, 10715–10722; (*e*) R. N. Grimes, *Carboranes*, Academic Press, Elsevier Inc., Amsterdam, 2011.

21 (*a*) K. Base, A. Petrina, B. Štíbr, V. Petricek, K. Maly, A. Linek and I. A. Zakharova, *Chem. Ind.*, 1979, 212; (*b*) M. A. Beckett, J. E. Crook, N. N. Greenwood and J. D. Kennedy, *J. Chem. Soc., Dalton Trans.*, 1984, 1427–1431; (*c*) J. H. Jones, J. D. Kennedy and B. Štíbr, *Inorg. Chim. Acta*, 1994, **218**, 1–3; (*d*) J. H. Jones, B. Štíbr, J. D. Kennedy and M. Thornton-Pett, *Inorg. Chim. Acta*, 1994, **227**, 163–166; (*e*) K. Baše, B. Štíbr and I. A. Zakharova, *Synth. React. Inorg. Met. – Org. Chem.*, 1980, **10**, 509–514; (*f*) T. K. Hilty, D. A. Thompson, W. M. Butler and R. W. Rudolph, *Inorg. Chem.*, 1979, **18**, 2642–2651; (*g*) M. J. Carr, T. D. McGrath and F. G. A. Stone, *Organometallics*, 2008, **27**, 2099–2106; (*h*) S. K. Boocock, N. N. Greenwood, M. J. Hails, J. D. Kennedy and W. S. McDonald, *J. Chem. Soc., Dalton Trans.*, 1981, 1415–1429; (*i*) M. G. S. Londesborough, C. O'Dowd, J. Bould, S. A. Barrett, C. A. Kilner, M. Thornton-Pett and J. D. Kennedy, *J. Chem. Crystallogr.*, 2000, **30**, 283–289; (*j*) B. Štíbr, K. Base, T. Jelinek, X. L. R. Fontaine, J. D. Kennedy and M. Thorntonpett, *Collect. Czech. Chem. Commun.*, 1991, **56**, 646–656; (*k*) Y. H. Kim, A. Brownless, P. A. Cooke, R. Greatrex, J. D. Kennedy and M. T. Pett, *Inorg. Chem. Commun.*, 1998, **1**, 19–22; (*l*) Faridoon, O. N. Dhubhghaill, T. R. Spalding, G. Ferguson, B. Kaitner, X. L. R. Fontaine and J. D. Kennedy, *J. Chem. Soc., Dalton Trans.*, 1989, 1657–1668.

22 J. H. Jones, X. L. R. Fontaine, N. N. Greenwood, J. D. Kennedy, M. Thornton-Pett, B. Štibr and H. Langhoff, *J. Organomet. Chem.*, 1993, **445**, C15–C16.

23 J. Bould and R. Macías, *J. Organomet. Chem.*, 2014, **761**, 120–122.

24 S. Heřmánek, *Chem. Rev.*, 1992, **92**, 325–362.

25 J. Holub, B. Štíbr, J. D. Kennedy, M. Thornton-Pett, T. Jelinek and J. Plešek, *Inorg. Chem.*, 1994, **33**, 4545–4552.

26 (*a*) R. N. Grimes, in *Comprehensive Organometallic Chemistry II*, ed. E. W. Abel, F. G. A. Stone and G. Wilkinson, Pergamon, Oxford, 1995, vol. 1, pp. 373–430; (*b*) R. N. Grimes, in *Comprehensive Organometallic Chemistry*, ed. G. Wilkinson, F. G. A. Stone and E. W. Abel, Pergamon Press Ltd, Oxford, 1982, vol. 1, ch. 5.5, pp. 459–542; (*c*) R. Macías, J. Bould, J. Holub, J. D. Kennedy, B. Štíbr and M. Thornton-Pett, *Dalton Trans.*, 2007, 2885–2897; (*d*) R. Macías, J. Bould, J. Holub, B. Štíbr and J. D. Kennedy, *Dalton Trans.*, 2008, 4776–4783.

27 J. Bould, J. E. Crook, N. N. Greenwood, J. D. Kennedy and M. Thornton-Pett, *J. Chem. Soc., Dalton Trans.*, 1990, 1441–1450.

28 K. Baše, M. G. H. Wallbridge, X. L. R. Fontaine, N. N. Greenwood, J. H. Jones, J. D. Kennedy and B. Štíbr, *Polyhedron*, 1989, **8**, 2089–2090.

29 J. A. Osborn and G. Wilkinson, *Inorg. Synth.*, 1967, **10**, 67–71.

30 Bruker, *SAINT-PLUS (Version 6.01)*, M. Bruker AXS Inc., WI, 2001.

31 G. M. Sheldrick, *SADABS Program for Correction of Area Detector Data*, University of Göttingen, Göttingen, Germany, 1999.

32 G. M. Sheldrick, *Acta Crystallogr., Sect. A: Fundam. Crystallogr.*, 2008, **64**, 112–122.

33 M. J. Frisch, G. W. Trucks, H. B. Schlegel, G. E. Scuseria, M. A. Robb, J. R. Cheeseman, G. Scalmani, V. Barone, B. Mennucci, G. A. Petersson, H. Nakatsuji, M. Caricato, X. Li, H. P. Hratchian, A. F. Izmaylov, J. Bloino, G. Zheng, J. L. Sonnenberg, M. Hada, M. Ehara, K. Toyota, R. Fukuda, J. Hasegawa, M. Ishida, T. Nakajima, Y. Honda, O. Kitao, H. Nakai, T. Vreven, J. A. Montgomery Jr., J. E. Peralta, F. Ogliaro, M. Bearpark, J. J. Heyd, E. Brothers, K. N. Kudin, V. N. Staroverov, R. Kobayashi, J. Normand, K. Raghavachari, A. Rendell, J. C. Burant, S. S. Iyengar, J. Tomasi, M. Cossi, N. Rega, J. M. Millam, M. Klene,

J. E. Knox, J. B. Cross, V. Bakken, C. Adamo, J. Jaramillo, R. Gomperts, R. E. Stratmann, O. Yazyev, A. J. Austin, R. Cammi, C. Pomelli, J. W. Ochterski, R. L. Martin, K. Morokuma, V. G. Zakrzewski, G. A. Voth, P. Salvador, J. J. Dannenberg, S. Dapprich, A. D. Daniels, Ö. Farkas, J. B. Foresman, J. V. Ortiz, J. Cioslowski and D. J. Fox, *Gaussian 09 (Revision A.02)*, Gaussian, Wallingford, CT, 2009.

34 N. Tsoureas, M. F. Haddow, A. Hamilton and G. R. Owen, *Chem. Commun.*, 2009, 2538–2540.